Winter Heat Content and Summer Stratification in Lake Superior

A THESIS
SUBMITTED TO THE FACULTY OF THE GRADUATE SCHOOL
OF THE UNIVERSITY OF MINNESOTA
BY

Kaitlin Boedigheimer

IN PARTIAL FULFILLMENT OF THE REQUIREMENTS
FOR THE DEGREE OF
MASTER OF SCIENCE

JAY AUSTIN

December, 2024

Acknowledgements

I would like to sincerely acknowledge and thank the following individuals for their support and encouragement:

- My research advisor, Dr. Jay Austin
- Thesis committee members, Dr. Katie Schreiner and Dr. Sam Kelly
- Staff and students at UMD
- Faculty and staff at LLO
- The Blue Heron research vessel and its crew
- My friends and family

Abstract

The Large Lakes Observatory has deployed subsurface moorings in Lake Superior since 2005. Temperature data from these moorings is used to construct complete subsurface thermal profiles for most years between 2005-2022. Total lake heat content, which is a function of temperature and depth, is computed from this data in order to analyze heat flux in Lake Superior and gain further insight on winter heating influences of summertime surface warming. Relationships among winter seasonal characteristics such as heat content, ice cover, and air temperature are explored using linear regression techniques. From surface water temperature data, yearly date of summer stratification is determined to examine connections with winter heat content and ice cover. Analysis of fit parameters indicates that winter heat content holds the stronger relationship, and it is shown to be a reliable predictor of summer stratification timing.

Contents

List of Tables

List of Figures

Chapter 1

Introduction

The Laurentian Great Lakes are the world's largest expanse of freshwater. They hold 84% of North America's freshwater and 21% of the global total (EPA, 2023), and are sizeable enough to influence local climate conditions. Freshwater from these lakes provides drinking water for 30 million people living along the surrounding coastlines (Krantzberg and Boer, 2008), which boast a greater total length than oceanic coastline bordering the contiguous United States (Gronewald et al., 2013). Anthropogenic global warming is impacting the Great Lakes Basin in several direct ways, including but not limited to perennially increasing surface water temperatures (Trumpickas et al., 2009), decreasing ice cover, (Mason et al., 2016; Ozersky et al., 2021; Austin and Colman, 2007), larger water level fluctuations (Gronewold et al., 2013), and increased duration of the summer stratified season (Austin and Colman, 2008; Anderson et al., 2021).

Lake Superior, the largest freshwater lake on Earth by surface area and the second largest by volume (Matheson and Munawar, 2009), has been singled out in several studies as the fastest-warming lake by many measures. In 2008 it was reported that surface water temperatures (SWT) in Lake Superior had risen by

3.5°C over the last century, doubling the rate of increase in local air temperature (Austin and Colman, 2008). It also has the highest rate of decline in ice cover of the Great Lakes at -0.42%/year for the period of 1979-2006 (Austin and Colman, 2007) as well as decreasing duration of its ice-covered season (-1 day/year). The discrepancy between rates of rising surface water temperatures and overlake air temperatures has been identified in other large, ice-covered lakes (O'Reilly et al., 2015), indicating a possible connection between ice decline and rapid surface warming.

A hypothesis presented by Austin and Colman (2007) specifically links declining ice cover of Lake Superior with increased summer surface warming due to absorption of excess solar radiation that would otherwise be deflected in a process known as the "albedo effect". Supporting evidence cited is a correlation between lake ice cover and timing of summer stratification - when less ice cover is present, the lake tends to stratify earlier than in years with more ice coverage, leading to more surface heating in the summer. Figure 1.1 displays the correlations from this study between ice cover and stratification onset as well as ice cover and summer SWTs.

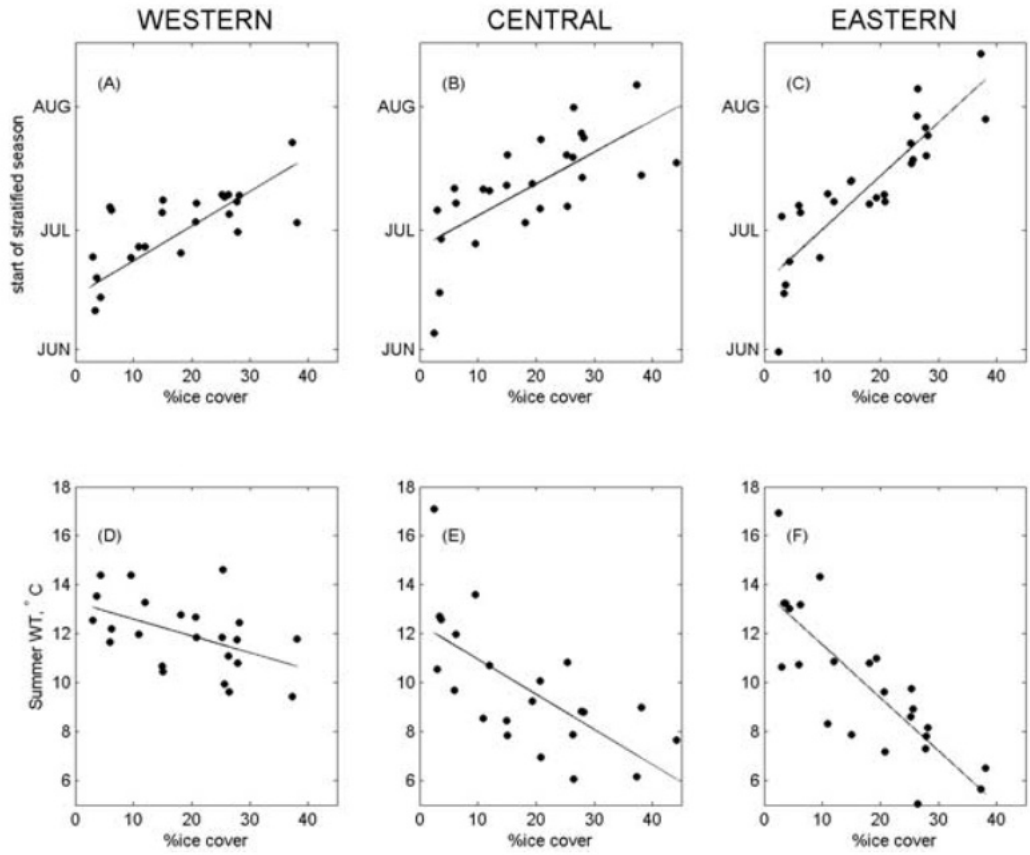

Figure 1.1: Yearly average lake ice cover vs. the start of summer stratification (top) and summer surface water temperatures (bottom) for 3 locations in Lake Superior. Figure from Austin and Colman (2007).

While moderate correlations between ice cover and these factors are evident, some doubt has since been cast over the importance of ice in lake heating processes. Researchers examined several ice-free lakes in California and Nevada, finding similar discrepancies in summer warming rates of surface water and air temperature as that of the ice-covered lakes (Schneider et al., 2009). They concluded that declining lake ice cover is not an essential driver of increasing rates of summer surface warming. This study was limited to satellite data, which was improved

upon in a 2015 analysis that used combinations of in-situ and satellite data to examine heating influences of 235 lakes across the globe. It was found that warming rates of lakes around the world do not depend on a shared singular factor such as location or ice cover, but that differing combinations of local conditions are responsible. In ice-covered lakes, which were observed as the fastest-warming, ice cover was re-confirmed as a key driver of rising summer SWTs. Rising air temperatures and stronger solar radiation was found to play a heavier role in the warming of ice-free lakes.

These results emphasize the need to evaluate lake heating characteristics on an individual-lake basis, as opposed to universally declaring or ruling out specific influences. In an attempt to separate various lake warming factors, analysis focusing on the Great Lakes during the 1997-1998 El Niño event utilized numerical modeling to explore several possible drivers. Extra wintertime heat accumulation was found to be a key influence of the extreme summer surface warming seen in Lake Superior, and it was again proposed that ice cover played a minimal role. It was further stated that declining ice cover along with earlier summer stratification is simply a reflection of milder winters (Zhong et al., 2016).

The two theories - causation vs. correlation of ice cover with rising summer surface water temperatures - are not mutually exclusive; it is likely that ice decline is both a result of increasing winter air temperatures while also lending to the acceleration of lake heating. However, the degree of ice's influence is difficult to evaluate since surface water temperatures and the formation of ice are both directly influenced by air temperature at the surface. There is also the added complication of opposing effects from the trapping of heat due to the insulation of ice cover, and excess warming from decreased presence of ice.

It's clear that the various heating mechanisms of the Laurentian Great Lakes,

which are some of the fastest-warming lakes of the world (Schneider and Hook, 2010), require more extensive and individualized treatment. There are many possible heating influences and difficulties involved in their analysis; the best way to cumulatively represent the effects from all possible factors is through total lake heat content. Measures of heat content involve the thermal profiling of the entire water column, data of which has been largely lacking for the Great Lakes. The largest subsurface water temperature (SSWT) dataset exists for the southern portion of Lake Michigan, maintained by GLERL since 1991. Recent analysis on this thirty-year dataset has revealed that rising deep water temperatures resulting from shorter winters lead to earlier summer stratification, and thus increased summertime warming (Anderson et al., 2021). This agrees with the connection established in the Zhong (2016) study, highlighting the importance of subsurface knowledge in evaluating lake warming trends - especially in large, deep lakes, where surface conditions are not representative of activity in deeper layers.

In 2005 scientists from the University of Minnesota's Large Lakes Observatory began deploying subsurface moorings in Lake Superior; at the time of writing there are 25 deployment records between 2005-2022. In 2014, a study of Lake Superior heat content compared patterns from three regions across the lake during the winter of 2009, revealing that higher amounts of ice cover in the Western region lead to a warmer spring season, thought to be a result of insulation from ice. It is speculated that the timing of ice cover dictates the direction of its influence on heat content, which more data from other high-ice years is needed to confirm (Titze and Austin, 2014). Analysis of winter heat content appears essential not only in characterizing warming trends but also in quantifying the weight of complicated seasonal influences such as ice cover on overall lake warming.

Freshwater is one of the world's most important resources; it is essential that

we understand the exchange of heat between our largest freshwater system and the continuously warming atmosphere. The most direct way to study the current state and future of the Great Lakes' response to global warming is through measures of their heat content and flux. In this thesis, we present analysis from the 25 years of SSWT data in the Western region of Lake Superior - the largest, coldest, and deepest of the Great Lakes. We focus on winter heat content and its relationship with the onset of summer stratification, and the role of ice cover on lake heating is re-examined. Net heat flux is quantified from these relationships and compared with predictions. In addition, we explore the memory of heat content and evaluate seasonal connections in order to form a more complete picture of year-round heating trends and what drives them.

Chapter 2

Theory

Here we discuss the theory involved in analyzing lake stratification, total lake heat content, and the heat exchange processes between a lake and the atmosphere in order to examine heat flux and winter seasonal influences of summertime warming in Lake Superior.

2.1 Lake Stratification

The formation of distinct thermal layers in a lake, known as stratification, is dictated by convection processes and the properties of density of water. Generally in a fluid, dense material sinks while lighter material rises due to gravity and pressure. As heat flows in or out of the lake, temperature redistributes through the layers of the water column in order to maintain stability. Normally the density of water is a nonlinear function of temperature and pressure; if we assume constant pressure, it can be estimated as

$$\rho(T) = 999.96 - 6.97 \times 10^{-3}(T - 3.985)^2 \tag{2.1}$$

This function is shown in Figure 2.1 across a typical temperature range of Lake Superior. Eq. 2.1 is referenced in Austin et al. (2011).

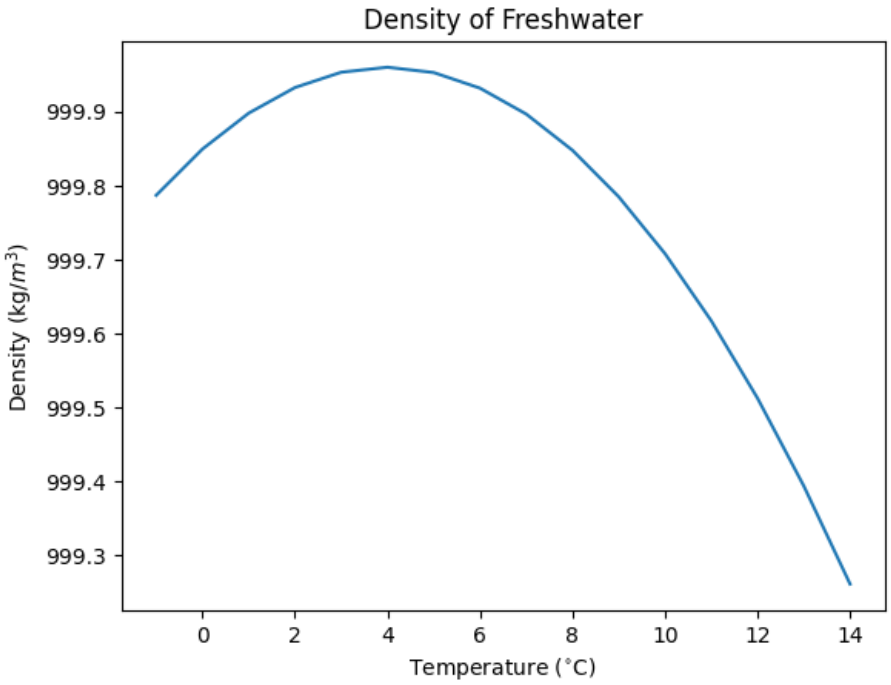

Figure 2.1: Density of freshwater as a function of temperature (assuming constant pressure).

From this we can see that the temperature of maximum density, T_{MD}, is about 4°C. This important parameter dictates the thermal structure and stratification of a lake - the deepest layers consist of the densest material closest to T_{MD}, growing either warmer toward the surface during summer (positive stratification) or colder during winter (negative/inverse stratification).

Lakes can be divided into three categories according to their stratification properties: holomictic, meromictic, and amictic. Patterns of stratification can vary widely both between and within a lake depending on factors such as latitude, size, and local climate/environmental characteristics. Most lakes are holomictic,

which means they stratifiy at least once per year. Meromictic lakes do not experience intermixing of layers, and a few lakes are amictic; mostly in Antarctica, amictic lakes are typically characterized by year-round ice cover and are inversely stratified. There are three types of holomictic lake mixing regimes; polymictic, dimictic, and monomictic. Lake Superior is a dimictic lake, meaning it stratifies twice a year. This is not the case for all of the Great Lakes; some of them see years with negative stratification and years without (Zhong 2016, Mason 2016).

Between the two stratified periods in Lake Superior are the spring and fall mixing seasons, where increased energy transfer in or out of the lake results in water temperature changes and thus mixing of layers. Outside of these mixing seasons, layers remain relatively stable/stratified, though weather events can cause brief and temporary mixing. For smaller, more shallow lakes such as Erie, such disturbances can disrupt stratification more significantly (Ozersky et al., 2021).

When stratified, a dimictic lake is comprised of three regions: the epilimnion, which is the surface layer, the midlayer or metalimnion, and the deepest layer known as the hypolimnion. Characteristics of these layers are defined by the stratification season and the size/location of the lake. During positive stratification in Lake Superior, the epilimnion is warm and shallow, growing colder through the metalimnion. The hypolimnion, which spans the bulk of the water column, forms a consistent temperature layer at T_{MD}. Negative stratification sees a thick, cold surface layer, with temperatures growing warmer with depth toward the hypolimnion, which is colder and less thick than during the summer.

The seasonal contrast in temperature and thickness of the layers is demonstrated in Figure 2.2 using two samples of Lake Superior temperature data; one from the winter/negatively stratified season (left) and then summer/positively stratified season (right) of 2019.

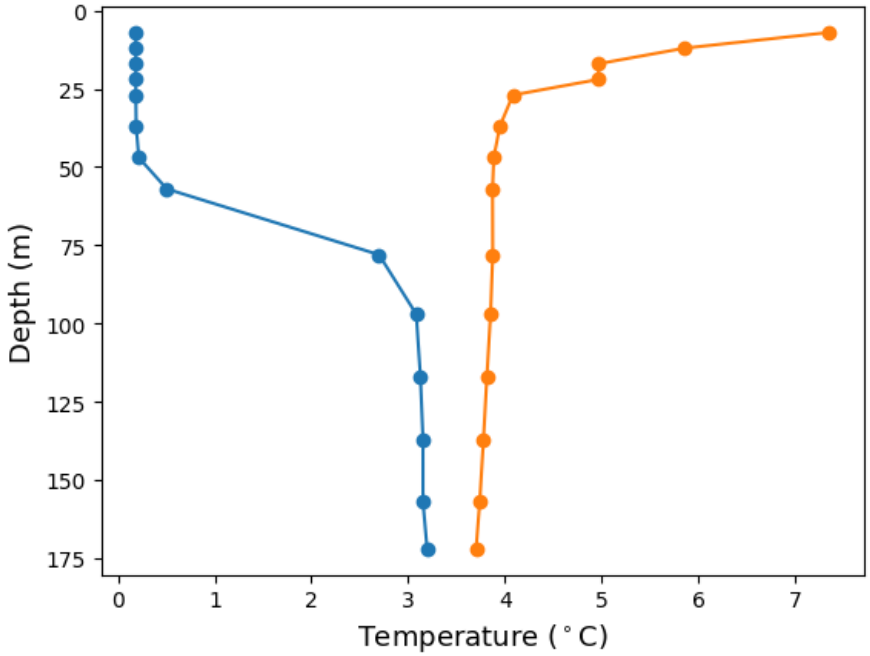

Figure 2.2: Temperature-depth profiles from the winter (left) and summer (right) stratified seasons of 2019. Data timestamps are 2019-02-18 and 2019-07-23.

It is evident from this graph that the surface layer is much thicker in the winter than in the summer, and temperature changes in the midlayer occur over a larger depth range.

It should be mentioned here that the constant pressure assumption used to approximate the density of water in Eq. 2.1 is not entirely accurate for a lake as deep as Superior. As pressure increases with depth, the temperature of maximum density decreases. This is noticeable in the deepest layers where T_{MD} is actually closer to 3.6°C (Titze and Austin, 2014), as evident by the bottom-most datapoints in Figure 2.2. However, our assumption is still a safe one for the purpose of this analysis - using the true density function vs. the constant-pressure estimation for heat content calculations results in negigible differences.

2.2 Heat Content

Heat content represents the amount of thermal energy stored in the lake. In order to define an equation from which heat content can be computed, we begin with the first law of thermodynamics - changes of internal energy in a system results from the work W done on or by the system, plus the amount of heat Q added to or taken from it. This is expressed conventionally as

$$\Delta U = Q + W \tag{2.2}$$

For a lake, the work term is negligible, so $\Delta U = Q$. This is the thermal energy which we call heat content. Switching the notation from U to H, we have $\Delta H = Q$. Heat Q is defined from specific heat capacity at constant pressure as

$$c_p = \frac{Q}{m\Delta T} \tag{2.3}$$

where m is mass and c_p for freshwater is 4,184 J/kg K. ΔT is the temperature measured with respect to a reference temperature, $\Delta T = T - T_{ref}$. Substituting these and using density as mass per volume, $\rho = m/V$, we rewrite in terms of ΔH as

$$\Delta H = \rho c_p (T - T_{ref}) V \tag{2.4}$$

For a lake system, we consider heat going into or out of each square meter of water and thus divide volume by area, leaving length L. So we have

$$\Delta H = \rho c_p (T - T_{ref}) L \tag{2.5}$$

and in order to calculate total lake heat content H, we integrate Eq. 2.5 across the water column. Assuming constant density and specific heat capacity, the continuous integral is

$$H = \rho c_p \int (T - T_{ref})\, dl \tag{2.6}$$

If we assume negligible advective current, there is no change in the horizontal direction, so the integral is one-dimensional in terms of vertical depth segments dz. We start at the surface ($z = 0$), integrating across the entire depth D:

$$H = \rho c_p \int_{-D}^{0} (T_z - T_{ref})\, dz \tag{2.7}$$

In determining choice of T_{ref}, it makes sense to use a limit such as 0°C or T_{MD}. We choose T_{MD}, as heat content computed this way will conveniently change signs with transitions between positive/negatively stratified seasons. Aside from usefulness, choice of reference temperature is arbitrary; differences will simply result in an offset in heat content calculations that disappears when considering changes in heat content.

Heat content will be calculated directly from discrete temperature data. Discretizing Eq. 2.7 and substituting our choice of T_{ref} as T_{MD} gives

$$H = \rho c_p \sum_{i}^{N} (T_i - T_{MD}) \Delta z_i \tag{2.8}$$

Heat content H is computed from each of N temperature measurements T_i at depth distance Δz_i from the last data point. Eq. 2.8 is the standard equation used in ocean heat content calculations (Dijkstra, 2008).

2.3 Surface Heat Fluxes

The exchange of heat between a lake and its surrounding atmosphere can be broken into four processes occurring at the boundary: shortwave radiation Q_{SW}, longwave radiation Q_{LW}, sensible heat flux Q_S, and latent evaporative flux Q_{LE}. Net heat flux is the sum of these four terms,

$$Q_{Net} = Q_{SW} + Q_{LW} + Q_S + Q_{LE} \tag{2.9}$$

each of which will be treated individually as follows.

2.3.1 Shortwave Radiation

Solar energy in the form of sunlight, or shortwave radiation, is the primary surface flux term that we will consider. Strength varies depending on latitude, cloud cover and time of year. Incoming clear-sky shortwave radiation values $Q_{SW_{in}}$ are estimated using the simplified equation

$$Q_{SW_{in}} = Q_0 cos\theta \tag{2.10}$$

where θ is the angle of the sun with the vertical, and Q_0 is the estimated amount of shortwave radiation at the top of the atmosphere. These terms are pre-calculated based on expressions from Appendix E of the U.S. Naval Observatory's 1978 Almanac for Computers. Note: using clear-sky values will result in maximal estimations of $Q_{SW_{in}}$.

Based on Eq. 2.10, the yearly cycle of daily average incoming shortwave radiation values in the Northern hemisphere is shown in Figure 2.3. Maximal shortwave radiation occurs during the summer solstice (June 20), and minimal amounts are reached during the winter solstice (December 21).

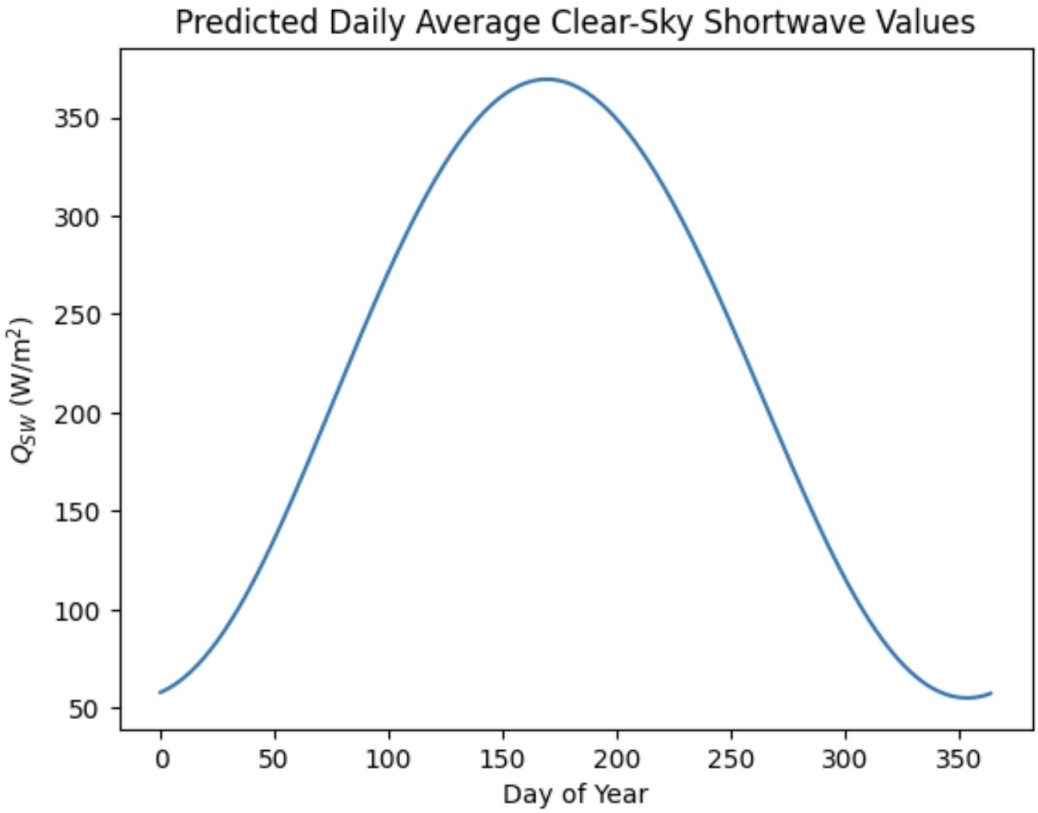

Figure 2.3: Yearly cycle of estimated clear-sky shortwave radiation.

When it hits the water's surface, a fraction of sunlight is deflected depending on the surface's albedo, known as the "albedo effect". The amount deflected is characterized by the surface type's albedo constant a. For freshwater, approximately 7% of sunlight is reflected ($a_w = 0.07$). Ice reflects a greater amount of sunlight, thus it has a higher albedo constant a_{ice}, ranging anywhere from 20-40% or up to 80% for ice covered with snow.

Total absorbed shortwave energy $Q_{SW_{net}}$ is then the difference between the incoming and outgoing terms,

$$Q_{SW_{net}} = Q_{SW_{in}} - Q_{SW_{out}} \tag{2.11}$$

where $Q_{SW_{out}}$ is approximated as the portion deflected due to the albedo effect. There are other less important factors involved in the amount of sunlight absorbed (such as water turbidity) that will not be considered here.

The amount of deflected shortwave without the presence of ice is represented in equation form as $Q_{SW_{out}} = Q_{SW_{in}} \cdot (1 - a_{water})$. With I as the percentage of lake ice cover, the amount deflected due to ice is $Q_{SW_{in}} \cdot (I)(a_{ice})$. The total amount of shortwave radiation deflected due to the albedo of the lake (including ice cover) is then

$$Q_{SW_{out}} = Q_{SW_{in}} \cdot (1 - I)a_{water} + Q_{SW_{in}}(I \cdot a_{ice}) \tag{2.12}$$

Substituting this into Eq. 2.11 and simplifying, we have

$$Q_{SW_{net}} = Q_{SW_{in}} \cdot I \cdot (a_{water} - a_{ice}) \tag{2.13}$$

Predicted clear-sky values for $Q_{SW_{in}}$ shown in Figure 2.3 and daily average ice cover data are used to approximate the effect ice cover has on the amount of shortwave radiation that reaches the surface through deflection.

2.3.2 Longwave Radiation

Longwave (also known as infrared or blackbody) radiation is thermal energy emitted by an object. The upward/outgoing longwave component Q_{UL} emitted by the lake is a function of surface water temperature. The incoming/downward component Q_{DL} comes from water vapor in the surrounding atmosphere. Following Lofgren and Zhu (1999), the upward amount radiated from the lake is simplified per unit area as

$$Q_{UL} = \epsilon \sigma T^4 \tag{2.14}$$

where ϵ is the emissivity of the surface, which for a highly efficient material such as water can be approximated as $\epsilon = 1$.

The downward component is approximated as

$$Q_{DL} = \sigma T^4 (0.53 + 0.065 e_a^{1/2})(p + (1-p)(1-N)) \tag{2.15}$$

where σ is the Stefan-Boltzmann constant, e_a is pressure from water vapor in the atmosphere, p is a cloud cover coefficient constant, and N is the fractional cloud cover amount. Though measures of total net heat flux will account for it, the amount of longwave radiation received at the lake's surface is complex to estimate, thus we will not be directly computing values in this study.

2.3.3 Sensible and Latent Heat Flux

Sensible (Q_S) and latent (Q_{LE}) heat fluxes are evaluated as

$$Q_S = \rho c_p \mid U_A - U_W \mid \theta \tag{2.16}$$

$$Q_{LE} = \rho L \mid U_A - U_W \mid q \tag{2.17}$$

with air density ρ, heat capacity of air c_p, and latent heat of evaporation L. U, θ and q are functions of velocity, temperature, and humidity difference, respectively. Sensible heat flux is a diffusive process that occurs due to vertical temperature gradients near the water's surface. It is taken to be negative when the surface water temperature is warmer than the air, and positive when the water is cooler. Latent heat flux is an evaporative process that depends on humidity level.

Monthly estimations of turbulent (senasible/latent) and net flux terms for each of the Great Lakes can be found in Lofgren and Zhu (1999); Table 2.1 displays these values for Lake Superior, where positive values represent flux into the lake.

Table 2.1: Monthly Estimations for Sensible, Latent, and Net Flux Terms (W/m^2) - Lake Superior (Lofgren and Zhu, 1999)

Month	**Latent**	**Sensible**	**Net Flux**
January	-69.565	-122.731	-254.844
February	-60.794	-105.989	-189.017
March	-34.222	-43.626	-17.797
April	-13.358	-5.327	101.857
May	-0.076	7.181	197.935
June	1.251	6.338	217.062
July	0.857	5.236	192.620
August	-9.928	1.501	144.585
September	-28.497	-7.843	54.081
October	-34.601	-17.142	-26.005
November	-57.732	-57.618	-144.521
December	-64.990	-82.618	-205.065

From Lofgren & Zhu (2000), the estimated annual cycle of sensible, latent, net radiative, and total net heat flux terms for Lake Superior is displayed in Figure 2.4.

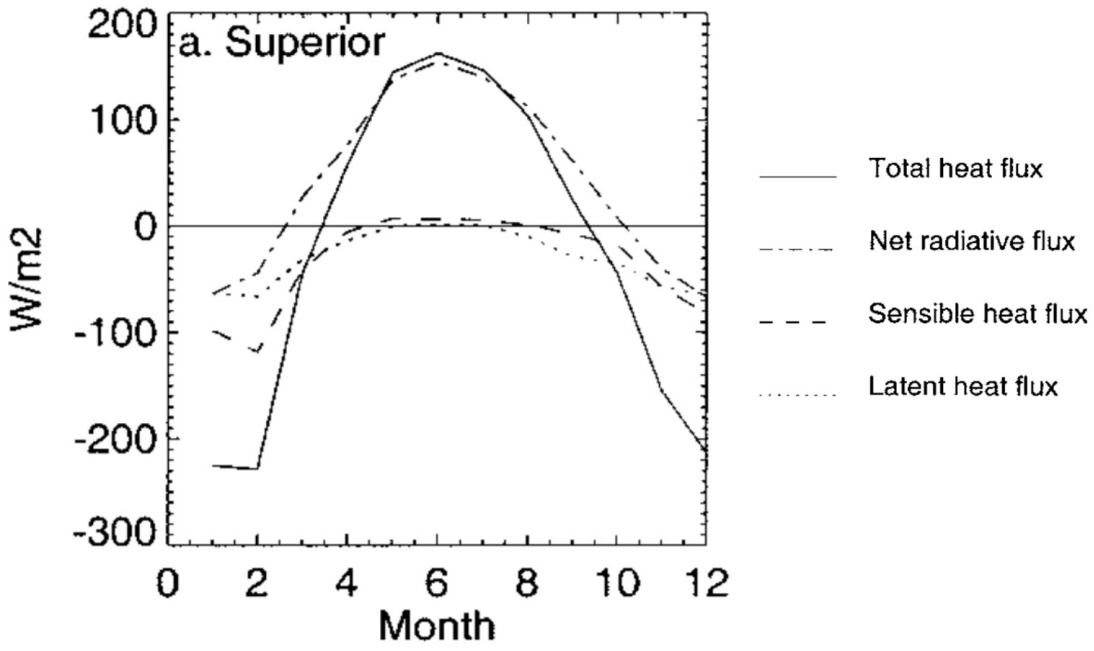

Figure 2.4: Annual cycle of surface heat flux terms in Lake Superior from Lofgren & Zhu (2000).

This estimated cycle and the monthly values of Table 2.1 will serve as a measure of comparison in our heat flux analysis.

The net total radiation received at the lake's surface is the sum of net shortwave energy $Q_{SW,net}$, the difference between upward and downward longwave radiation components $Q_{DL} - Q_{UL}$, and latent and sensible heat fluxes Q_{LE} and Q_S. Rewriting Eq. 2.9 accordingly, we have total net heat flux

$$Q_{Net} = Q_{SW,net} - Q_{UL} + Q_{DL} + Q_{LE} + Q_S \tag{2.18}$$

As opposed to analyzing terms individually, a more straightforward way of evaluating net heat flux is directly from changes in heat content over a time interval,

$$Q_{Net} = \frac{\Delta H}{\Delta t} \tag{2.19}$$

Equating this with Eq. 2.18, we hypothesize linear relationships between heat content and the factors embedded in the surface flux terms, such as air temperature and deflected shortwave energy due to ice cover.

Chapter 3

Data/Methods

Types of data involved in this analysis are surface water temperature from buoys, subsurface water temperature from moorings, air temperature taken on land, and satellite ice cover. A map of the relevant data collection sites across Lake Superior is displayed in Figure 3.1 for reference. There are three main buoy/mooring locations marked 45006/WM, 45001/CM, and 45004/EM. Air temperature data is from the Devil's Island land station marked DISW3.

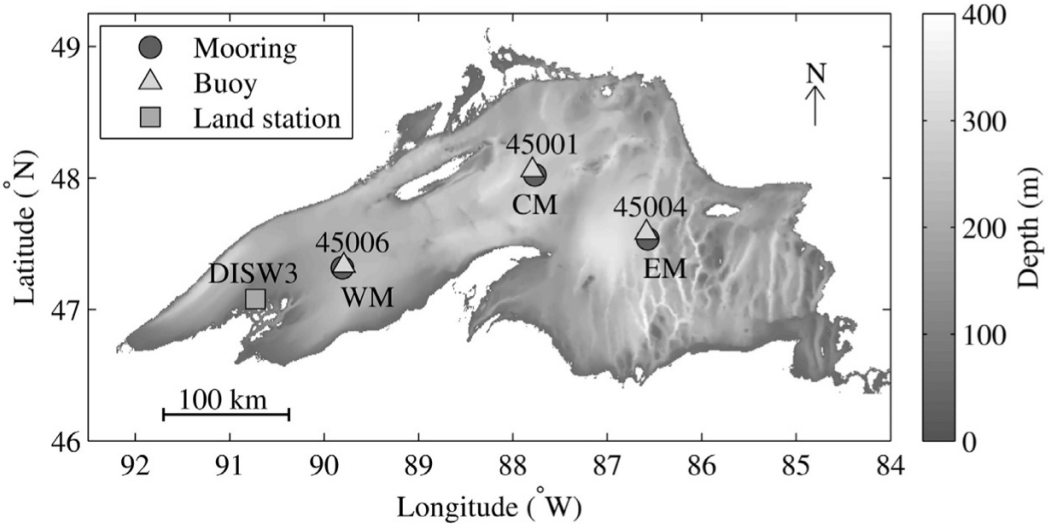

Figure 3.1: Gantt chart of data deployment stations across Lake Superior. (Figure from Titze and Austin, 2016)

The most complete surface and subsurface water temperature data records are from the Western region (45006/WM), so analysis will be largely focused on this data.

Obvious noise or missing data is removed, except in the case of the occasional small section of bad SSWT data from a faulty thermistor - these sections are interpolated via replacement with the previous thermistor's data. This is one admitted weakness of analysis; missing SSWT data should be replaced by averaging nearest values. However, these interpolated sections make up a very small portion of SSWT data. Sections of bad data that are large enough to produce outliers are omitted.

We hypothesize linear relationships and trends, so the bulk of analysis involves linear regression techniques and comparison of fit parameters. Correlation

coefficients are used to test the strength of linear relationships, and statistical significance is tested with p-values at a significance level of $\alpha = 0.05$. All calculations, graphs, and fits are done in Python.

3.1 Surface Water Temperature and Stratification

The National Data Buoy Center (NDBC) has deployed buoys to collect hourly surface water temperatures 1 m from the surface at several locations across Lake Superior since 1979. Buoy 45006 data is available since 1981; this complete record is shown in Figure 3.2 below.

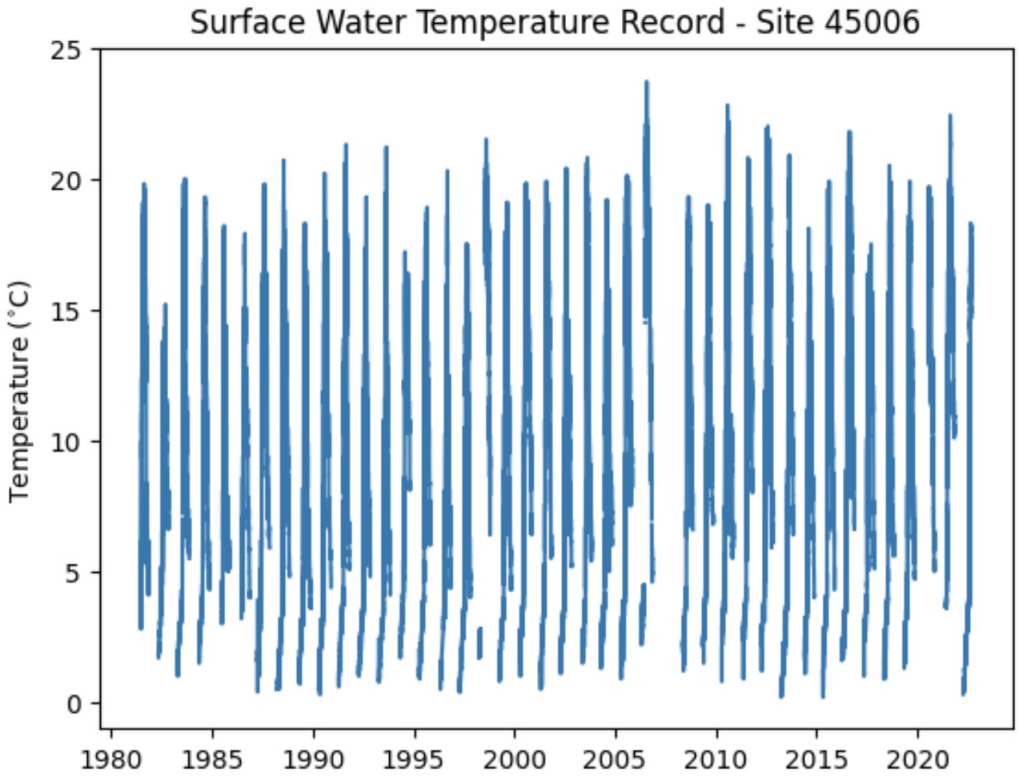

Figure 3.2: Complete hourly surface water temperature record from NDBC buoy 45006.

Buoys are deployed from May to November, which is the usual ice-free season of Lake Superior. As no winter data is available, relationships involving winter surface water temperatures will not be explored.

The main use of SWT data in this study is to determine yearly dates of summer stratification onset. The method of determining this is simple; the official start date is considered to be the first day where daily averaged surface water temperatures exceed T_{MD}. Before this point, the lake is transitioning from winter stratification where temperatures through the layers are cooler than T_{MD}. As heat is absorbed from increasing springtime solar radiation, mixing occurs as dense material sinks, and the entire water column heats up to T_{MD}. The surface reaches it last, signifying the beginning of positive stratification, and surface warming accelerates. In a lake as deep as Superior, layers generally do not re-mix until Fall.

Figure 3.3 demonstrates this transition in surface temperatures during the summer stratifying periods of years 2004 and 2006.

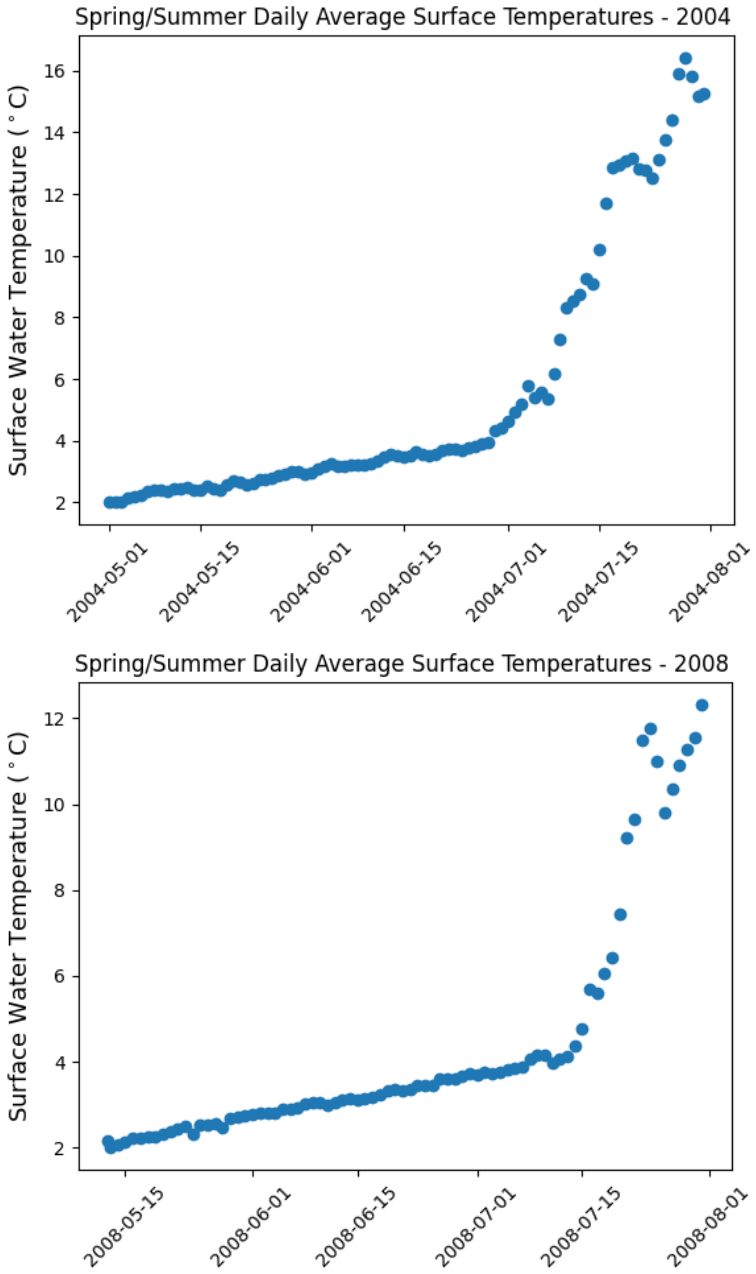

Figure 3.3: Daily averaged surface water temperatures for the spring-summer periods of years 2004 (top) and 2008 (bottom); buoy 45006.

Using this method, onset dates of summer stratification for most years between

1982-2022 are plotted below in Figure 3.4. A full table of stratification dates is included in Appendix C.2. There are data gaps in the summer of 1998 and most of June-July in 2006. Data is also missing for the entire year of 2007, 2020 before August, and 2022 after September. All years with significant missing summer data are excluded from stratification analysis. This includes the first year of data collection (1981), as the buoy was not deployed until after stratification.

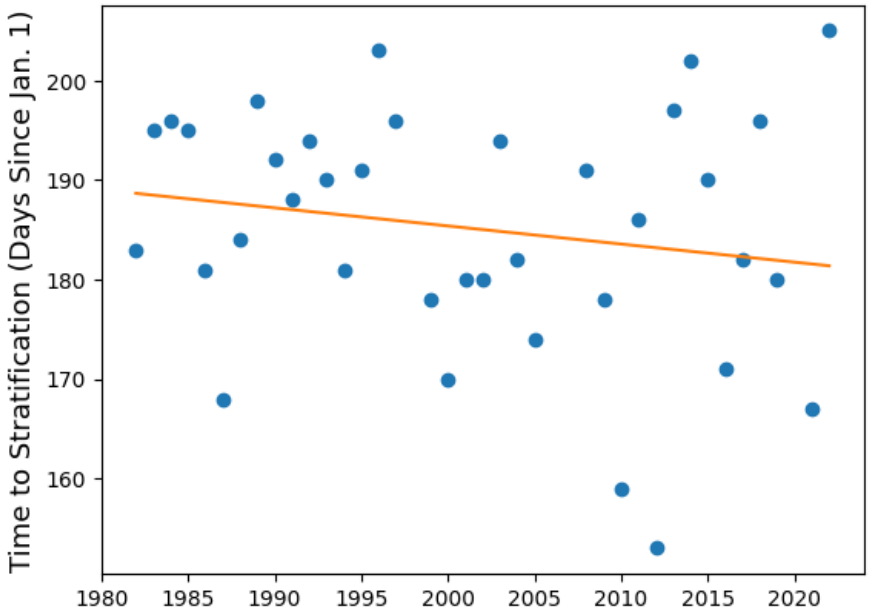

Figure 3.4: Lake Superior summer stratification dates determined using surface water temperature data from buoy 45006.

Though we focus on the buoy 45006/WM location, there is a fair amount of variation in stratification timing between the three main regions (Western, Eastern, and Central) which will now be presented and lightly discussed. Some of this variation is natural due to depth differences between regions; as the Western region is most shallow, it typically stratifies first, followed by Central and then Eastern. See Figure 3.5 for a colored bathymetry map of Lake Superior.

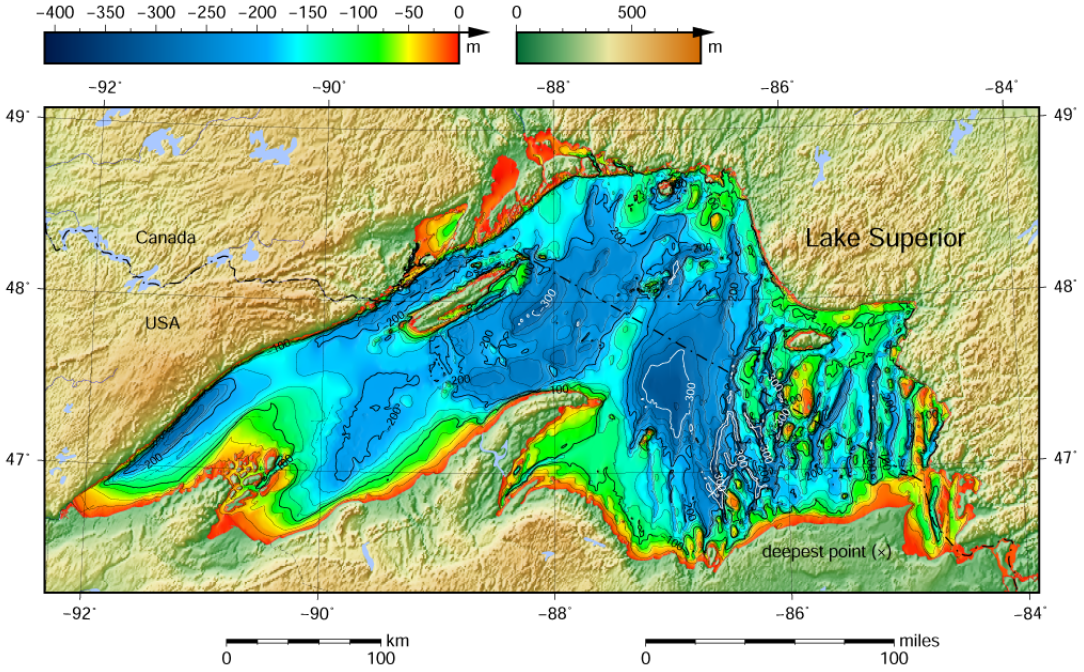

Figure 3.5: Lake Superior bathymetry map. Image source: wikimedia.org user Darekk2 (2015), `https://commons.wikimedia.org/wiki/File:Lake_Superior_bathymetry_map.png`.

Heat content and ice cover generally follow the same patterns, which will be discussed in more detail in the Results section.

Figure 3.6 shows the time to summer stratification at all three buoy sites, next to the difference in timing (in days) between the Central/Eastern and Western regions.

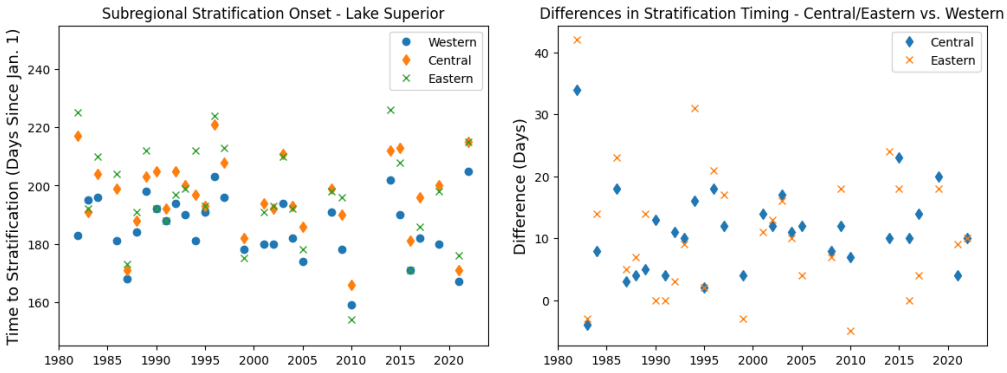

Figure 3.6: Left: Lake Superior summer stratification dates determined using SWT data from the Western (45006), Central (45001) and Eastern (45004) buoys. Right: Differences (in days) of stratification onset between Central/Eastern and Western.

A (usually) small portion of this variation can be attributed to the method of determining stratification date. While the first day above T_{MD} is marked as the official stratification date, and is usually followed by the steep increase that represents stratifying of the water column, sometimes temperatures fall back down for a short period before stratification truly begins. The resulting difference is normally not larger than a few days, except for in the case of the year with the largest subregional variation (the first year plotted, 1982).

SWT data from 1982 is shown below in Figure 3.7, first for the Western region and then the Central and Eastern. The dashed line indicates the stratification date as determined by the daily average algorithm.

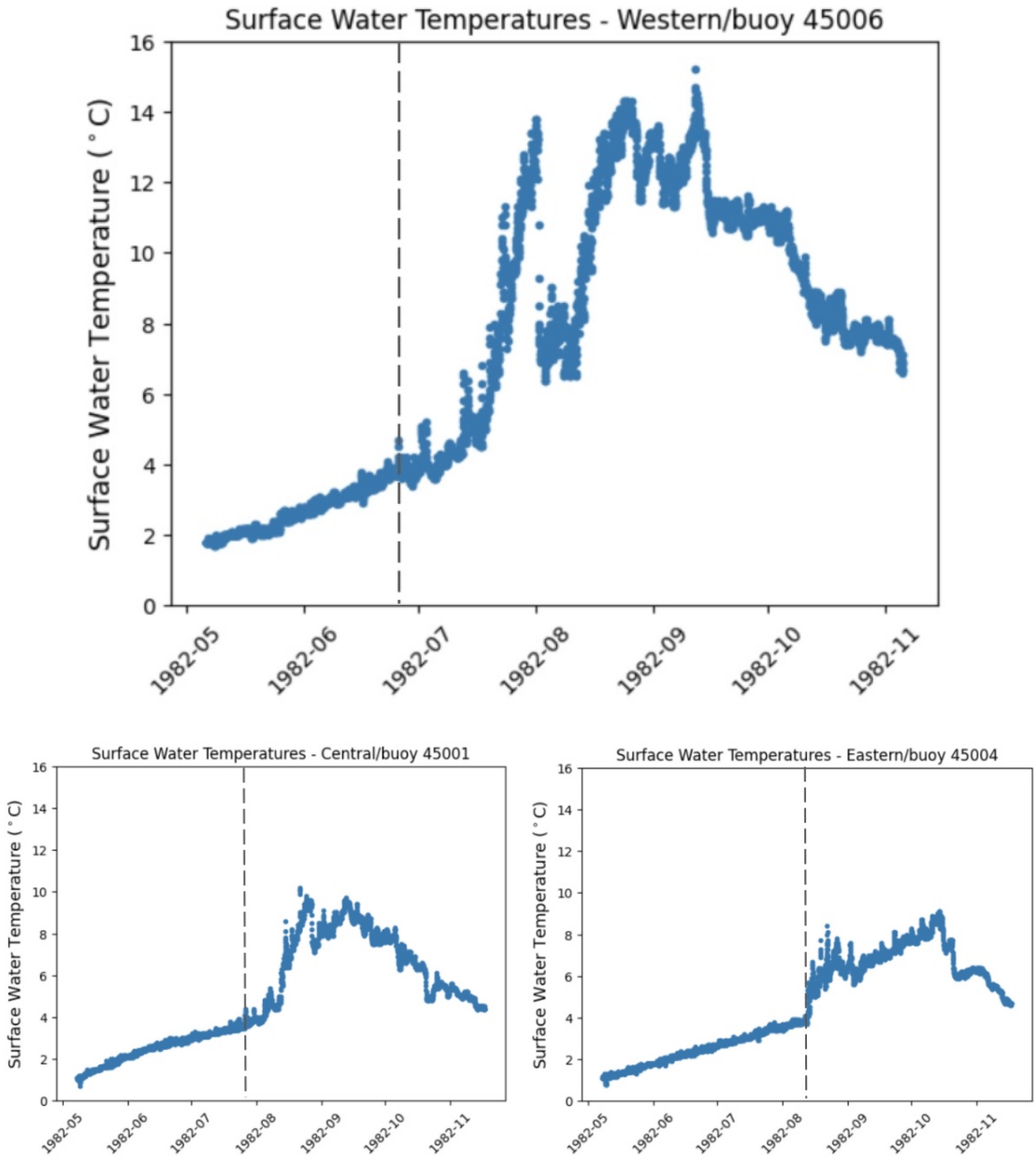

Figure 3.7: Top: SWTs from the year 1982 at buoy 45006/Western location. Bottom: SWTs from the year 1982 at buoys 45001/Central and 45004/Eastern.

In this year, SWTs at the Western site rise above T_{MD} and dip back down at least

twice before the water column actually stratifies in mid-July. The algorithm tags the stratification date as late June - a whole month earlier than stratification at the Central/Eastern locations. A more sophisticated algorithm would account for these instances, but again the difference is typically not as severe.

In general, summer stratification timing is correlated between the regions; comparing correlations at the Central/Eastern sites with Western (shown in Figure 3.8) confirms that the Central area tends to align more closely (r=0.83, p=3e-9) than the Eastern region (r=0.77, p=3e-7), though not by much.

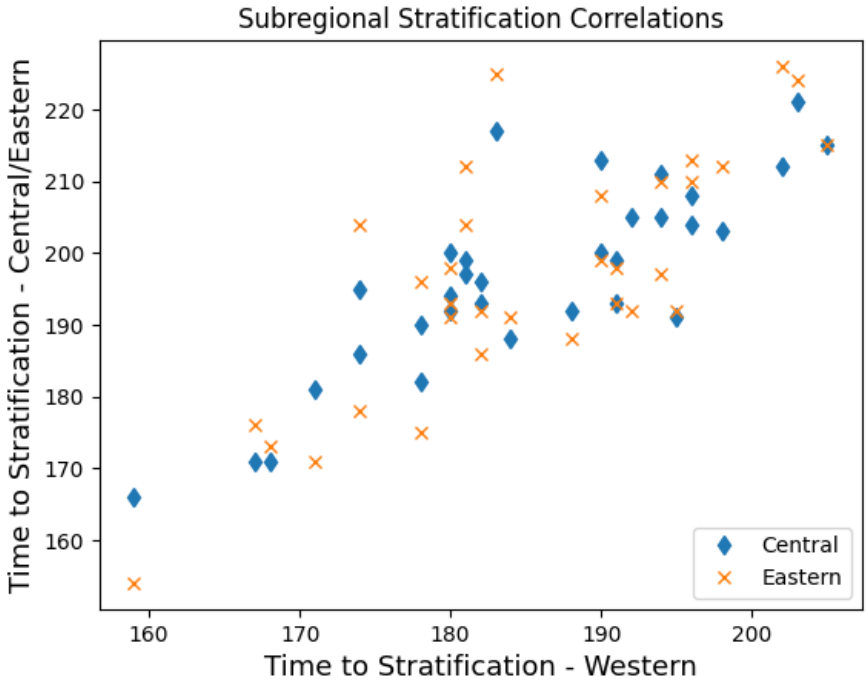

Figure 3.8: Correlations of time to stratification between the Central/Eastern and Western regions of Lake Superior.

Analysis of the relationship between winter heat content and summer stratification is independent of these subregional differences, as we will be comparing SSWT and SWT from the same region (Western). The air temperature data site is

conveniently closest to this location, justifying connections with air temperature.

3.2 Subsurface Water Temperature and Heat Content

The Large Lakes Observatory has deployed subsurface moorings across Lake Superior since 2005 to collect various kinds of data including SSWT, which is taken by strings of thermistors (resistance thermometers) attached to the moorings. The thermistors span the approximate length of the water column, spaced closer together toward the surface where temperature gradients tend to be larger, growing progressively further apart with depth. Most thermistor models used are RBR TR-SOLO3 and SOLO Ts. Temperature data is measured at a frequency of 1 Hz with an uncertainty of 1°C.

Individual plots of SSWT for each WM deployment can be found in Appendix B.2, with an example from the Fall 2013 deployment shown below in Figure 3.9. Deployments are labeled as spring or fall followed by the year. Exact seasonal deployment dates vary significantly between years depending on weather and availability of the research vessel/crew.

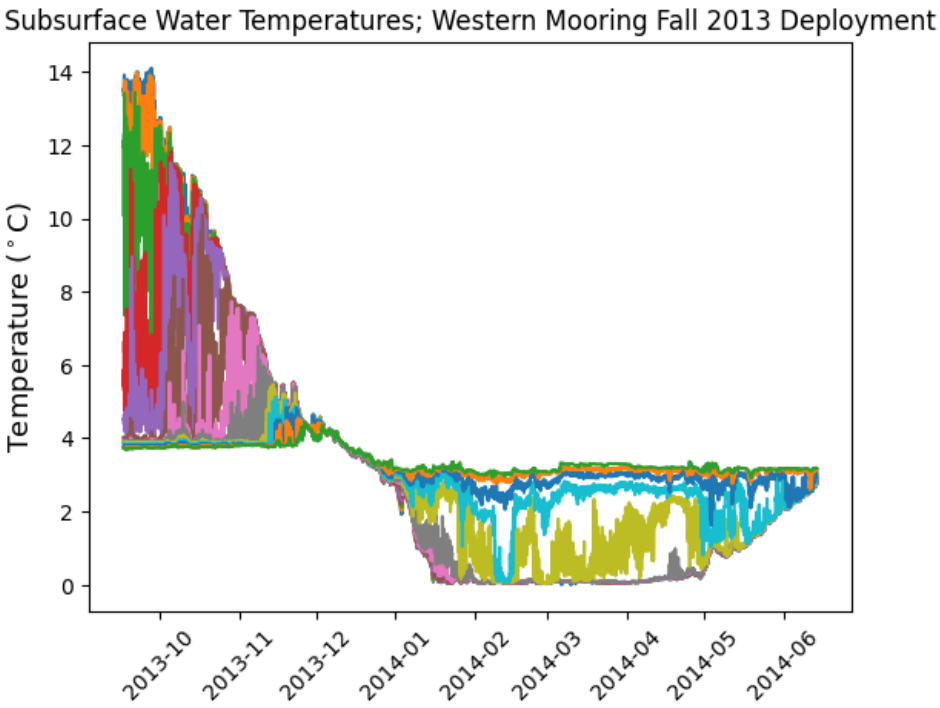

Figure 3.9: Subsurface water temperature profile from the WM Fall 2013 deployment. Various thermistor depths are represented by color.

There are multiple colors making up the subsurface temperature data that represent various thermistor depths. Most deployments used 10-15 thermistors, though the first two deployments used only 6 and Fall 2021 used 91. See Table C.1 in the Appendix for a full list of each deployment's number of thermistors used and their individual depths.

Figure 3.10 shows the complete record of SSWT data from the Western Mooring.

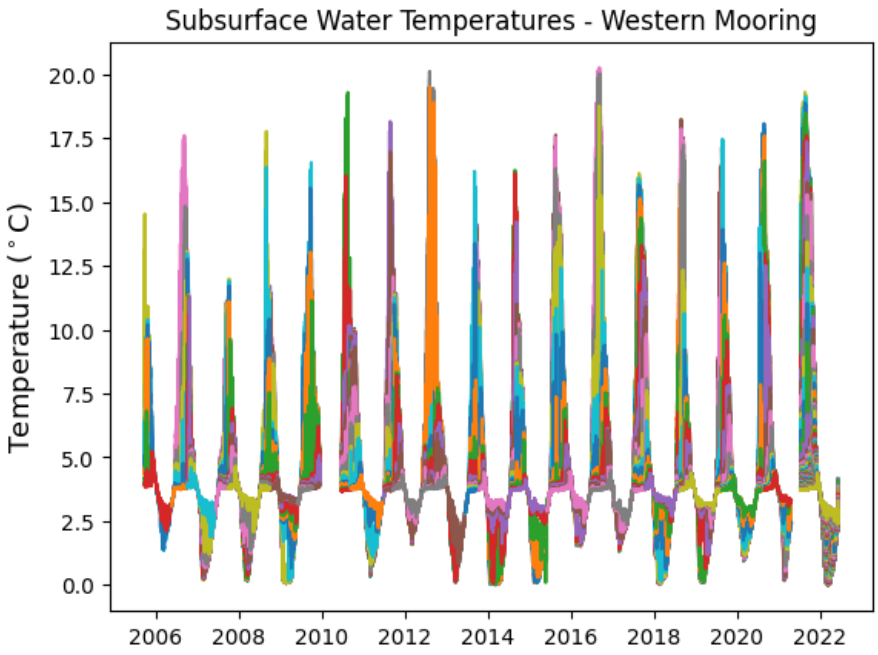

Figure 3.10: Complete subsurface temperature record from Western Mooring in Lake Superior.

This subsurface water temperature data is used to compute heat content according to Eq. 2.8. Again, heat content is analyzed primarily for the Western Mooring, since it has the most complete dataset of 25 deployments between the years 2005-2022, 23 of which have sufficient data to calculate heat content. There are a small handful of common deployment years at the Central and Eastern Moorings that will allow for a light comparison of heat content across the three regions.
The Fall 2005 and Fall 2009 deployment will be excluded from WM heat content analysis due to insufficient data.

Heat content calculated from all usable SSWT data at WM is shown in Figure 3.11. Units of heat content are Joules per square meter; graphs shown in this analysis are scaled to Gigajoules (1e9 Joules). Individual heat content plots for each WM deployment can be found in Appendix B.3.

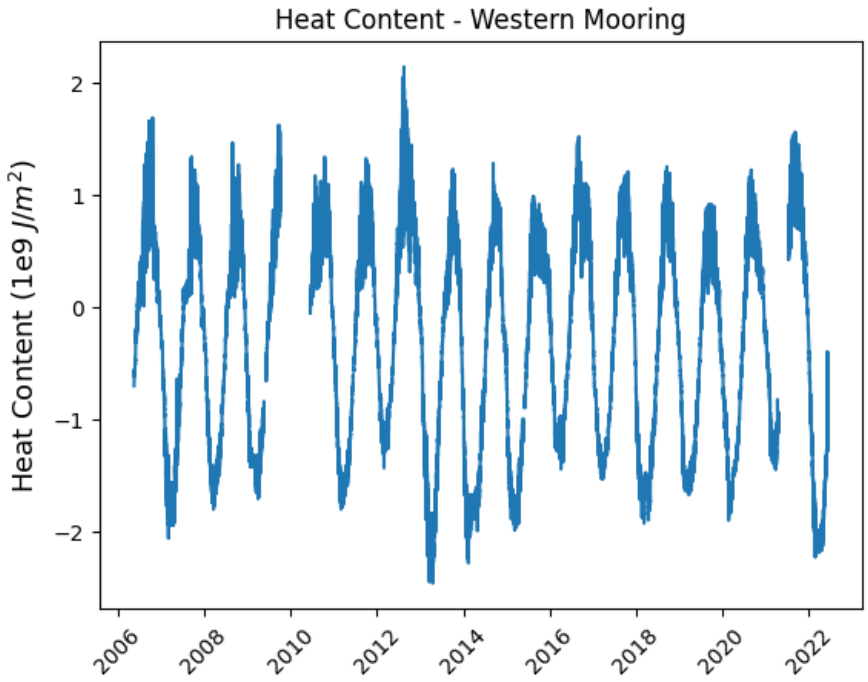

Figure 3.11: Heat content calculated from WM SSWT data between years 2006-2022.

Figure 3.11 highlights the winter and summer of 2012 as the mildest, and the subsequent winter of 2013 as the coldest (followed closely by winter 2014). Over the course of a year, heat content values range by up to 4 GJ; interannual variation of winter/summer seasonal values is around 1 GJ.

A closer look at heat content over the course of a year is shown for the Spring 2012 and 2016 deployments in Figure 3.12; heat content is displayed below the corresponding subsurface temperature plots, which are represented here by only the top, bottom and middle thermistors for clarity.

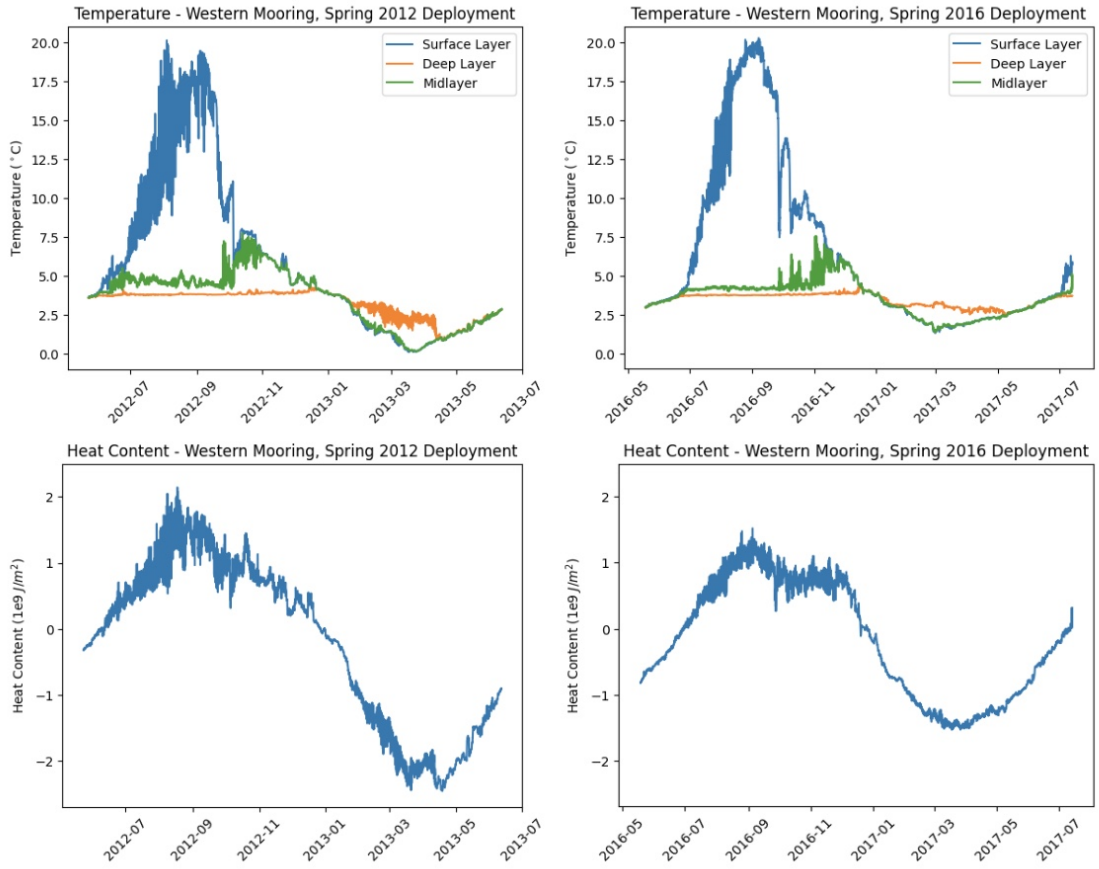

Figure 3.12: Top: three-layer temperature profiles for spring deployments 2012 (left) and 2016 (right). Bottom: Corresponding heat content calculated from the full array of temperature-depth data.

Much of the presented analysis will focus on winter heat content, where winter is chosen to be represented by averages across February/March. This is generally the coolest period of heat content in Lake Superior, as will be demonstrated. A few relationships/trends involving summer heat content are discussed as well, for which averages across August/September will typically be used. Occasional comparisons using single-month averages or other time periods are discussed when relevant.

3.2.1 Uncertainty in Heat Content Calculations

The largest uncertainty involved in calculating heat content comes from estimating temperature values between thermistors. There are a discrete number of depths from which temperature data is taken; the in-between values are unknown. However, there is a fixed possible temperature range due to the properties of stability - since density increases with depth, temperature between points must fall within the known values of the points. Visually, this range is represented by the boxes outlined by the left and right-side paths shown in Figure 3.13.

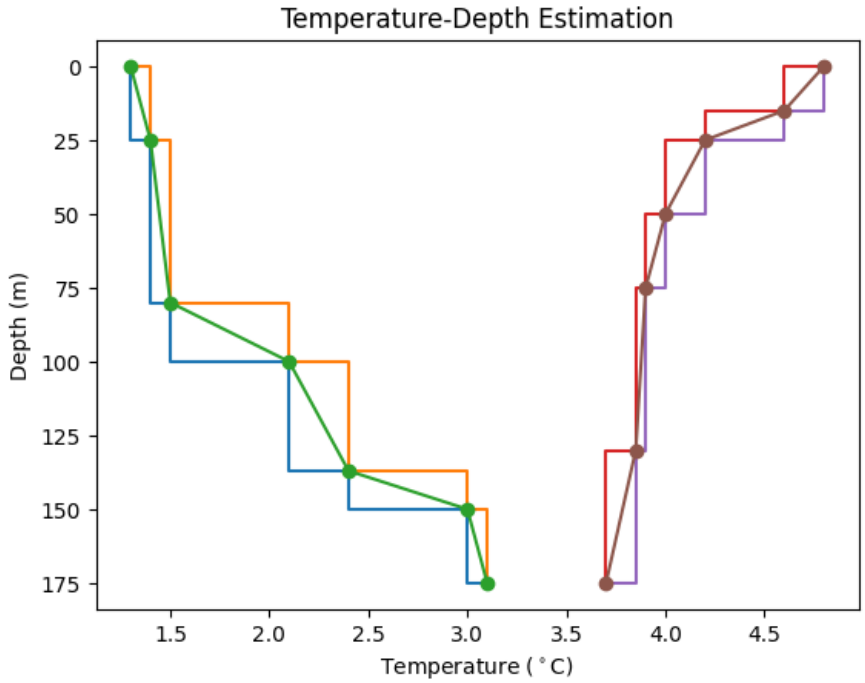

Figure 3.13: Example temperature-depth profile based on data from times a. Left: 2019-05-01 22:00:00; still negatively stratified and b. Right: 2019-07-12 14:00:00; positively stratified. The three possible interpolation paths between points are shown.

As heat content is the area under this curve, calculations will differ depending on which path is used to estimate values. Each path corresponds to a different

method of assigning Δz values in $T_i/\Delta z_i$ pairs when computing Eq. 2.8. Using the right-side path will give a maximal estimate of heat content during negative stratification (left profile of Figure 3.13), as this method includes more area at a warmer temperature, while the left-side values will underestimate. During positive stratification (right profile) they flip, with the right-side path now being the underestimation. We will be using the middle path method to calculate heat content, which averages the maximal and minimal possible temperatures at each point.

Figure 3.14 shows the variation in heat content calculations from all three interpolation methods for the Spring 2018 deployment.

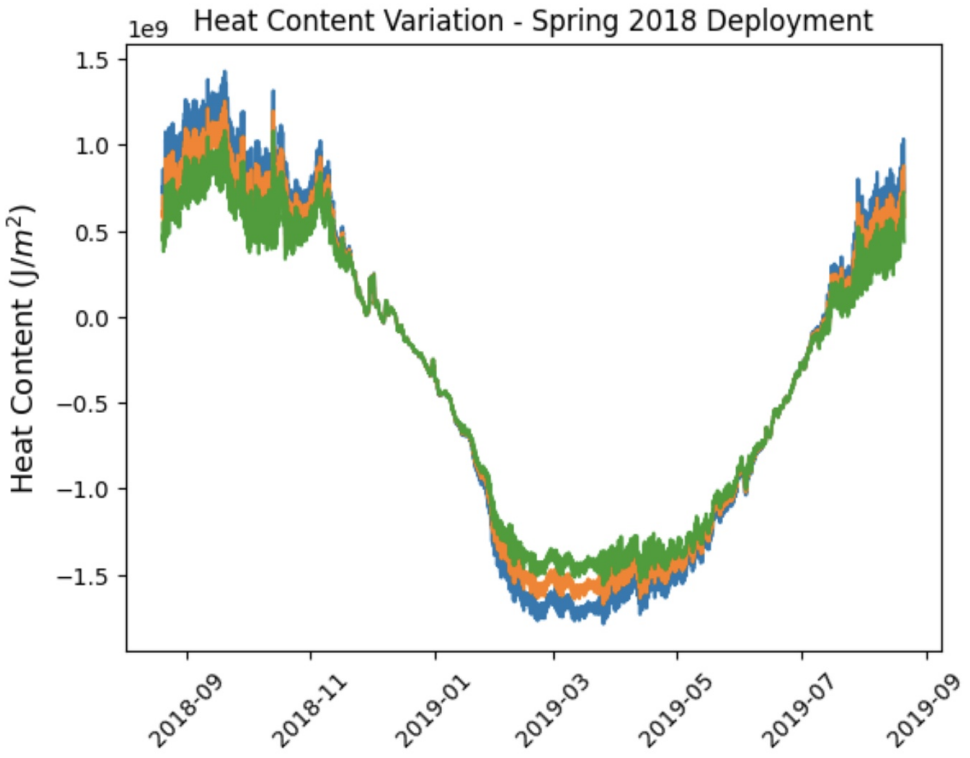

Figure 3.14: Heat content calculated using all three interpolation methods; Fall 2018 WM deployment.

From this graph, it can be seen that the annual variation of the heat content cycle (just over 3 GJ for this time period) is much larger than uncertainty from interpolating (around 0.5 GJ at most).

Figure 3.15 displays the variation in February monthly averages for each year, showing a similar spread in values of less than 0.5 GJ.

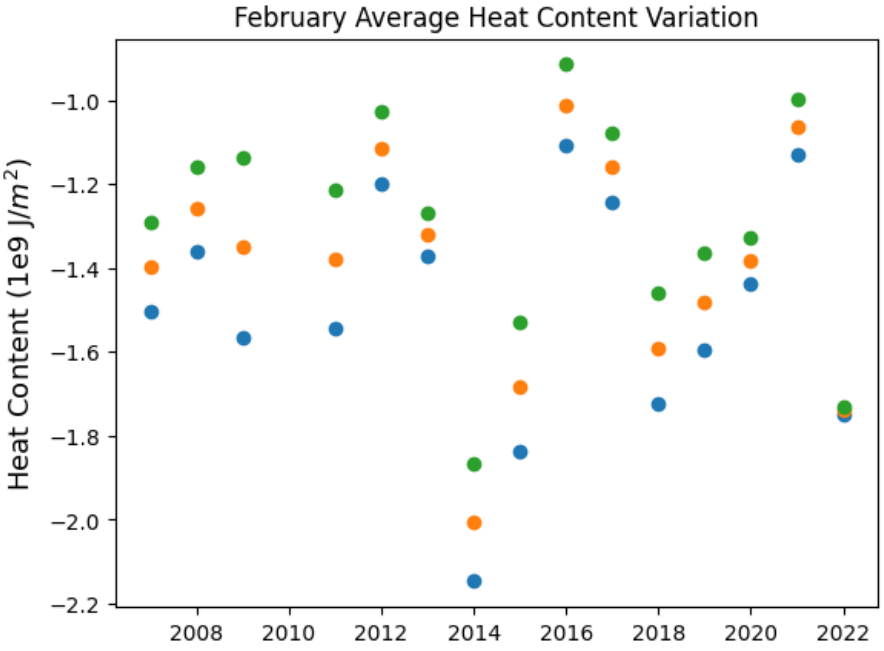

Figure 3.15: February average heat content calculations using all three interpolation methods.

Note the year of least variation, 2022, which corresponds to the year of 91 thermistors (vs. the usual 10-15). Of course, more data is the best way to reduce uncertainty - using more thermistors results in more known values spaced tighter across the water column, minimizing the amount of interpolation needed.

3.3 Ice Cover

Daily averaged satellite ice cover data from NOAA historical ice cover reports is available from 1972 onwards, displayed in Figure 3.16. This data represents fractional total lake ice coverage.

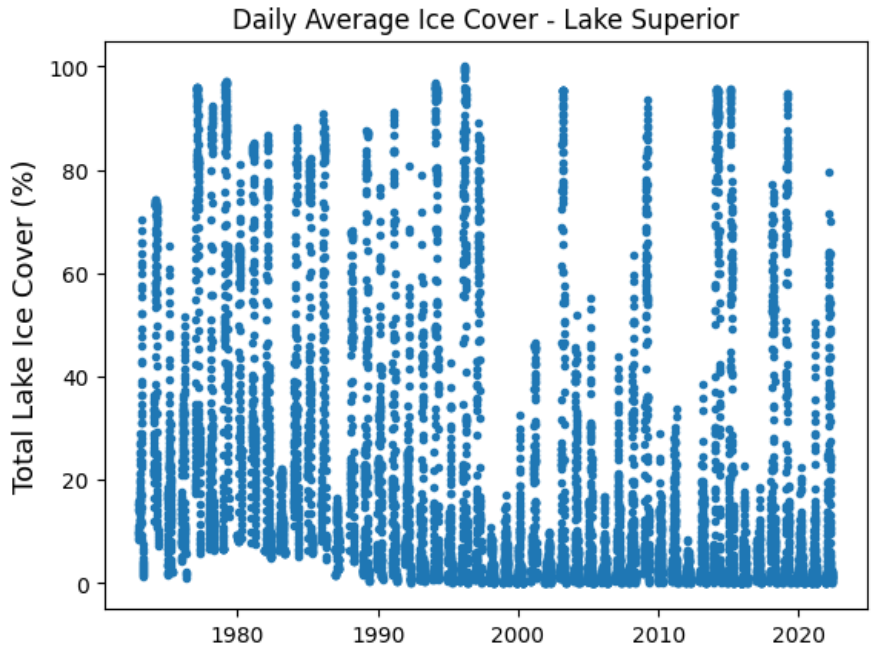

Figure 3.16: Daily averaged total lake ice cover.

Notable years of minimal ice cover are identified as 1998, 2002 and 2012.

This data will be used to calculate deflected shortwave radiation according to Eq. 2.12 in order to evaluate the effects of ice cover on lake heating and summer stratification. We acknowledge that ice cover formation varies across the lake, as will later be discussed. The region of focus is the western part of the lake, where ice forms first, so we will consider total lake ice cover to be representative of this location.

3.4 Air Temperature

Air temperature data is taken at several Coastal Marine Automated Network stations operated by the NDBC. We use data from Devil's Island (marked "DISW3" in Figure 3.1) which is relatively close to buoy 45006/WM. It should be noted that this station is located 192 m above sea level, and data is collected 25 m above the site elevation - in total, more than 200 m above SWT/SSWT data collection sites.

The complete record of DISW3 hourly averaged air temperature is shown in Figure 3.17.

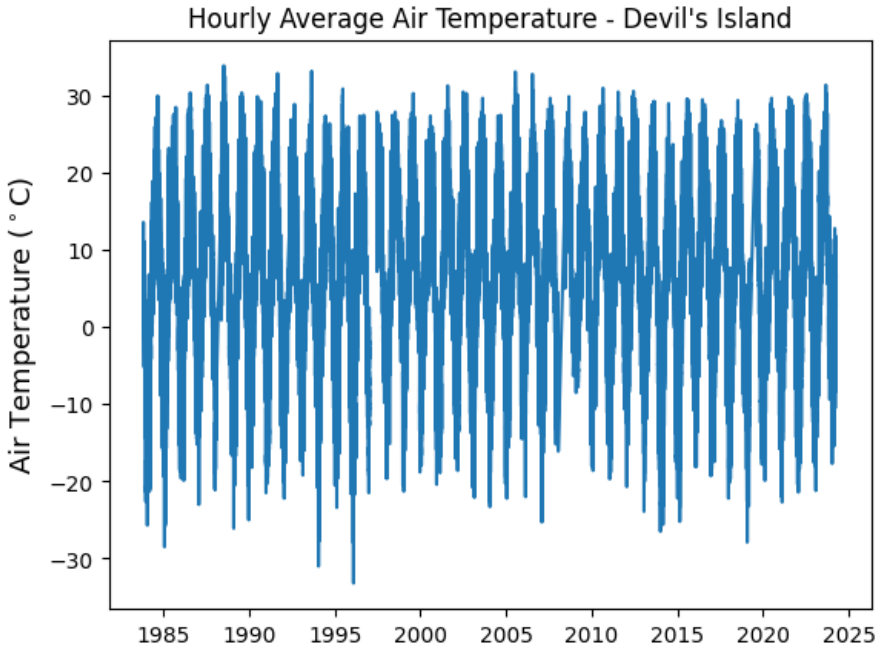

Figure 3.17: Hourly averaged air temperature from data taken at Devil's Island.

There are gaps in DISW3 air temperature data from January to July in 1997, from January to June in 2008, and for most of December 2008.

Chapter 4

Results

4.1 Heat Content

From 23 Western Mooring deployments between 2006-2022, daily averaged annual cycles of heat content in Lake Superior are shown in Figure 4.1.

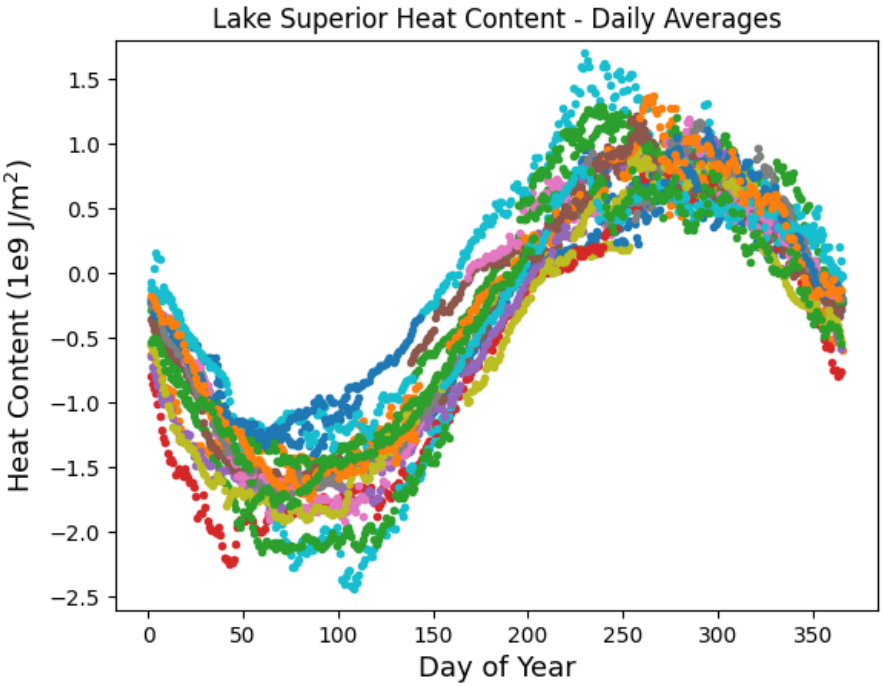

Figure 4.1: Annual cycles of daily average heat content, calculated from all available SSWT data between 2005-2022 at the Western Mooring in Lake Superior.

There are a few informative characteristics from this graph.

1. The rate of change in heat content during the winter to summer transition is fairly constant. This is evident from the similar slopes of the curves between days 100-225.

2. Winter variability is considerably larger than summer variability. The range of values is around 1 GJ for winter, and about half of that for summer (disregarding the topmost curve between days 200-250, which is the anomalously warm summer of 2012).

3. The annual cycle retains its shape from year to year.

Feature 2 is partially explained when considering the seasonal difference in the temperature structure of Lake Superior. Referring back to Figure 2.2, the surface layer is much thicker during the winter when the lake is negatively stratified than in the positively stratified summer season. Temperature changes occur at the surface, and heat content is the area under the temperature-depth curve, so the larger area of potential temperature difference during the winter results in a wider spread of possible heat content values. The shallower epilimnion of summer allows for less such variation; even when summertime surface temperatures are extreme, there is far less area affected.

Figure 4.2. shows the annual heat content cycle in terms of monthly averages.

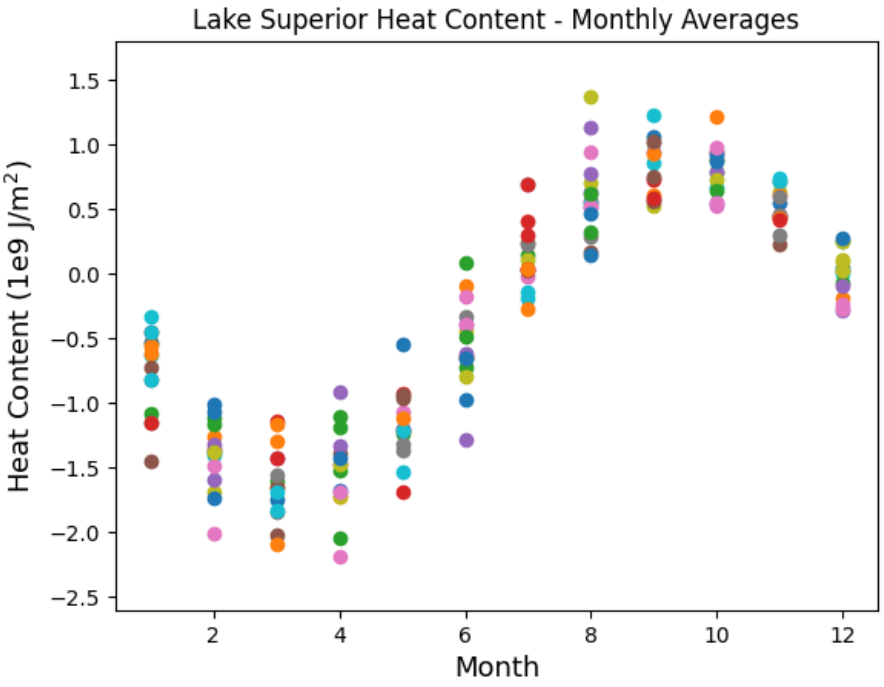

Figure 4.2: Monthly average heat content in Lake Superior for all WM deployments between 2005-2022.

From the monthly plot it is again evident that the coldest months in the lake

(February, March) exhibit larger variation than the warmest months (September, October). In addition to the structural difference in temperature between seasons, this may reflect air temperature conditions as well as the variability of ice cover leading to differing rates of springtime surface warming.

Early winter appears to be the period of greatest consistency, which may simply be another result of the thin summer surface layer - as air temperatures drop, heat available to be transferred out of the lake is lost quickly since it is already at the surface. At this time surface heating processes are relatively straightforward and free from the complications of ice cover, which is usually not present in substantial amounts until January (see Figure 4.14).

One last feature to note is the wide range in values of April-August, which is largely due to contributions from the outlying daily average curves.

Generalizing further to look at possible seasonal trends, summer and winter average heat content over the period of 2006-2022 is plotted in Figure 4.3. Here summer is represented by averaging across August-September, and winter is February-March.

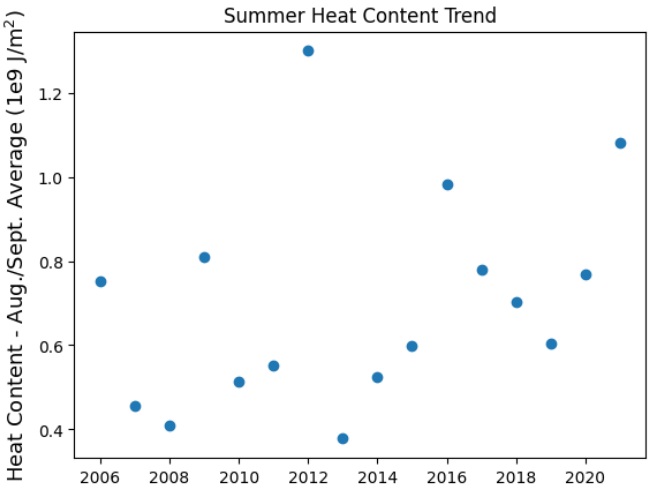

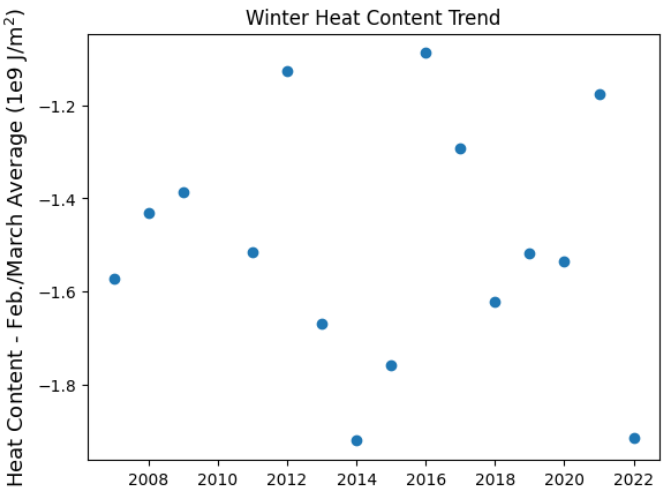

Figure 4.3: Summer and winter seasonal average heat content in Lake Superior.

There is not a defined trend in either season. Summer averages may be on the rise, but the fitting parameters from current data are too weak to confirm this (r=0.34, p=0.2), and winter is weaker still (r=-0.09, p=0.74). These results aren't dependent on the time period of evaluation - restricting to single months such as February for winter or using different combinations such as September/October for summer produces even weaker results. The lack of a trend in seasonal heat content could be due to data limitations, but if there was a long-term memory of heat content, we would expect to see some evidence here.

The memory of the system can be further examined by looking at autocorrelations. First, from all deployments' daily and monthly average heat content values, the mean is computed and removed to show the complete record of heat content anomalies. The daily/monthly mean annual cycle and mean-centered heat content averages over the years is shown in Figure 4.4.

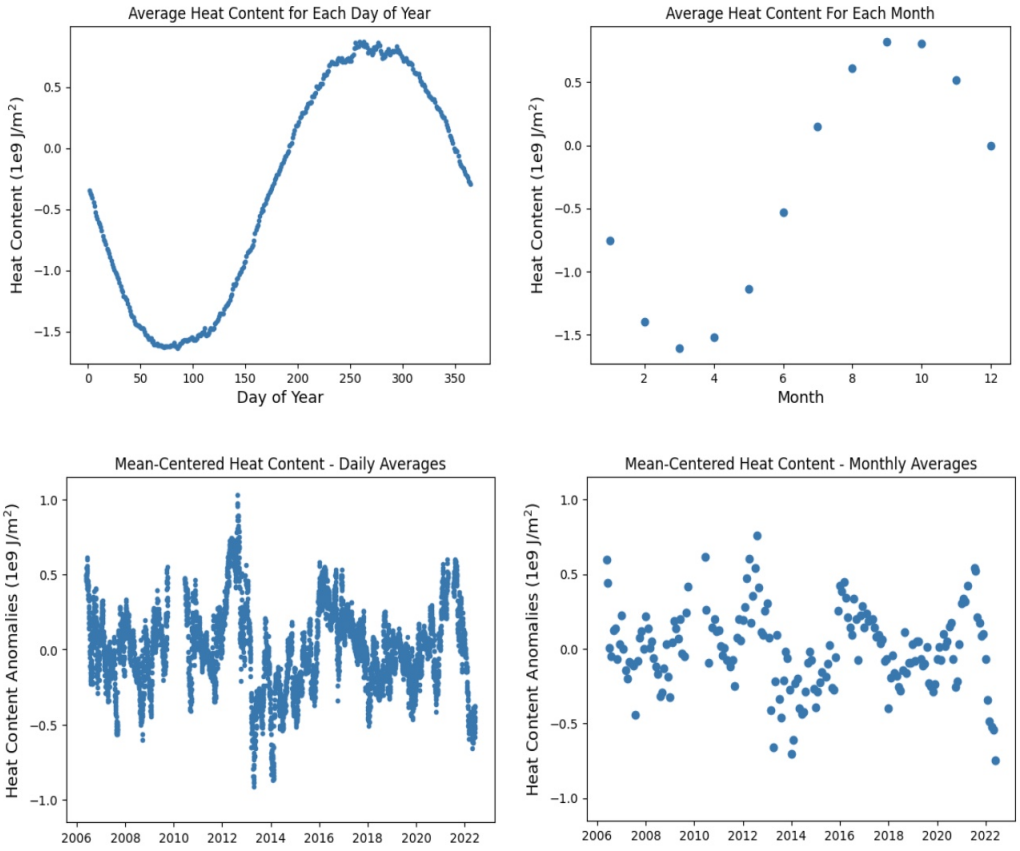

Figure 4.4: The mean annual cycle calculated across all deployments' daily (top left) and monthly (top right) averages; mean-subtracted daily (bottom left) and monthly (bottom right) average values plotted across the entire WM deployment record.

The mean cycles further highlight the weight of outlying data, most noticeable in the daily plot's jump at 250 days and in the low monthly value of April. Even though February is usually a colder month, April's average is lower due to two significant outliers.

The anomaly plots are too noisy to provide much information on their own, but there is a noticeable difference in heat content levels before and after the extremes seen in 2012-2013.

To compute autocorrelations, the anomalies are shifted over time and the covariance from each shifted dataset is divided by the sample variance from the mean. This gives a series of correlations vs. shift/lag, which is shown in Figure 4.5. Correlation values start at 1 (0 lag) and decrease as the data is shifted over more time. The point where it reaches 0 represents the extent of the memory.

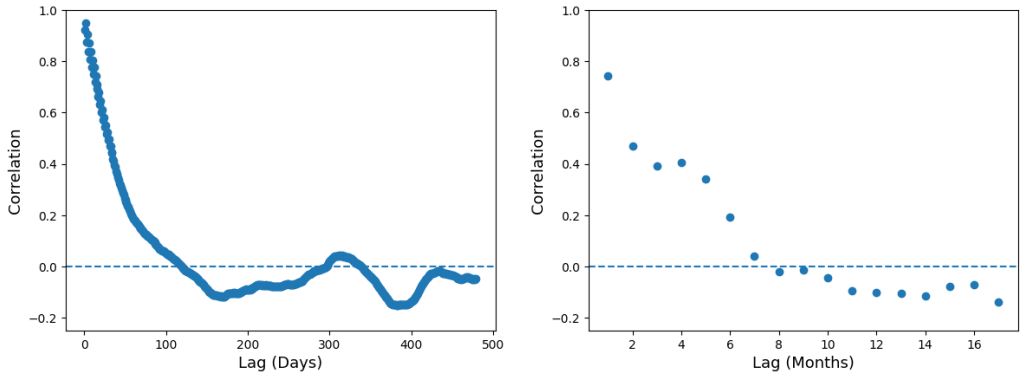

Figure 4.5: Autocorrelation of daily and monthly heat content in Lake Superior.

The correlation goes to zero at about 7 months, which says that heat content has essentially no influence on future values past half of a year. Larger shifts are characterized by noise fluctuations between -0.2 and 0.2.

To compare whether the memory has a seasonal preference, the relationships between winter-to-summer heat content with summer-to-winter, plotted in Figure 4.6. According to linear fitting parameters, winter heat content appears to have a much stronger influence on following summer values (r=0.77, p=0.001) than summer has on winter (r=-0.16, p=0.57), though the summer-to-winter parameters improve significantly when evaluating instead as a September/October average (r=-0.47, p=0.07).

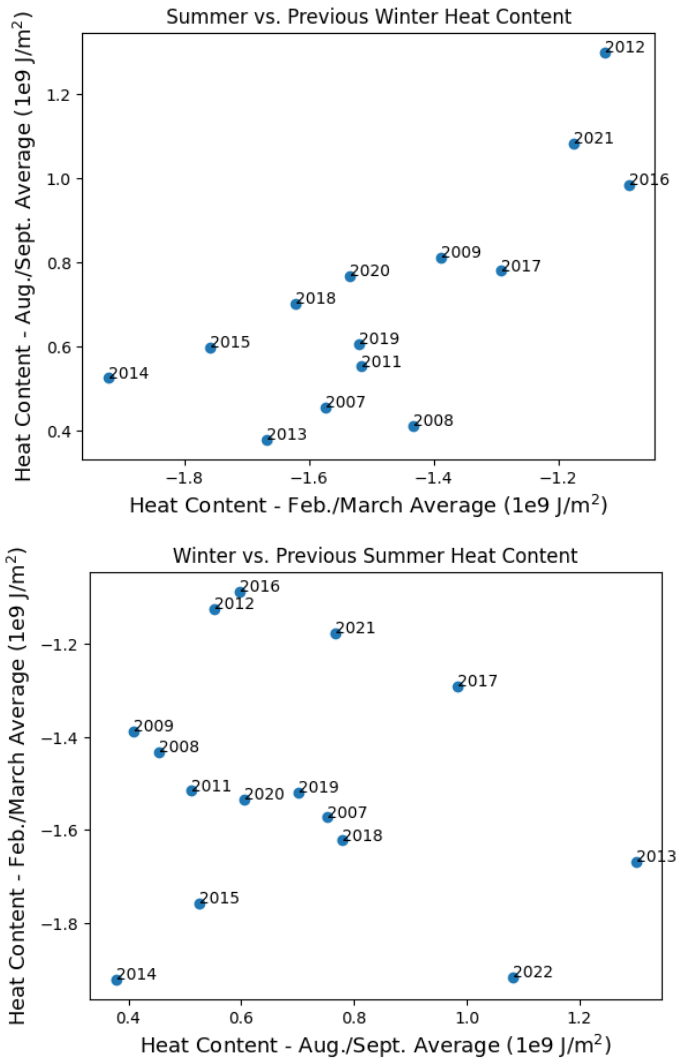

Figure 4.6: Relationships between winter and following summer heat content (top); summer and following winter (bottom).

The strength of the winter-to-summer connection is a promising lead into the main purpose of this dissertation - determining the predictive power of winter heat content on the timing of summer stratification.

We now report the strongest link found in this study, which is between winter heat content and the onset of subsequent summer stratification. This relationship

is shown in Figure 4.7. It is negatively linear, with a correlation value of r=-0.9 and p-value of 3e-05. Data is limited, but this correlation is remarkably strong. The association is intuitive - when there is more wintertime accumulation of heat in the lake, stratification takes place earlier in the summer, and vice versa.

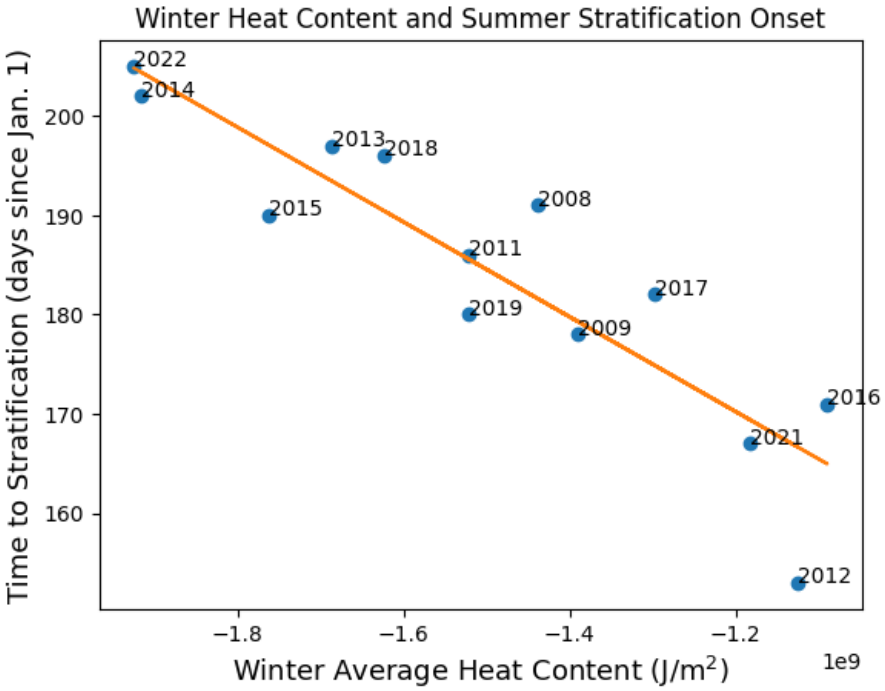

Figure 4.7: Onset of summer stratification in Lake Superior as a function of winter average heat content.

Further physical insight can be obtained from this plot. The change in heat content over a period of time is heat flux, represented by the reciprocal of the slope of Figure 4.7. The slope itself is -4.77e-08 J/m^2/day; taking its reciprocal and converting appropriately (using 1 Watt=1 Joule/second and 1 day=86,400 seconds), net heat flux based on this graph is about -243 W/m^2. This can be interpreted as each additional day of delay in summer stratification equating to an extra 243 W/m^2 of outgoing heat flux.

A reference of comparison is the net heat flux estimations from Lofgren and Zhu (1999). There are several weaknesses of this study; heat flux predictions are based on surface conditions alone, and data is only available across 3 years (1992-1995). The winter months of January, February and March are further restricted to the single year of 1995 due to a reported lack in quality data. Net heat flux predictions from a single winter season's surface data obviously aren't ideal representations. These values are also obtained using the assumption of an ice-free surface, which the paper admits is a "major weakness" resulting in roughly estimated values for January-March in Lake Superior.

Keeping these limitations in mind, the net flux estimations from Lofgren and Zhu (1999) are listed in Table 2.1 as -189 W/m^2 for February and -17.8 W/m^2 for March. Both of these represent considerably less outgoing flux than the amount represented by our data in Figure 4.7. Aside from methodical differences, a possible explanation for our larger outgoing flux values is related to effects of ice cover.

4.2 Ice Cover

The declining trend in Lake Superior annual average ice cover is shown in Figure 4.8. The slope represents a decrease in ice cover of $0.49 \pm 0.13\%$ per year for the time period of 1971-2022, which agrees with previous literature values (Austin and Colman, 2007).

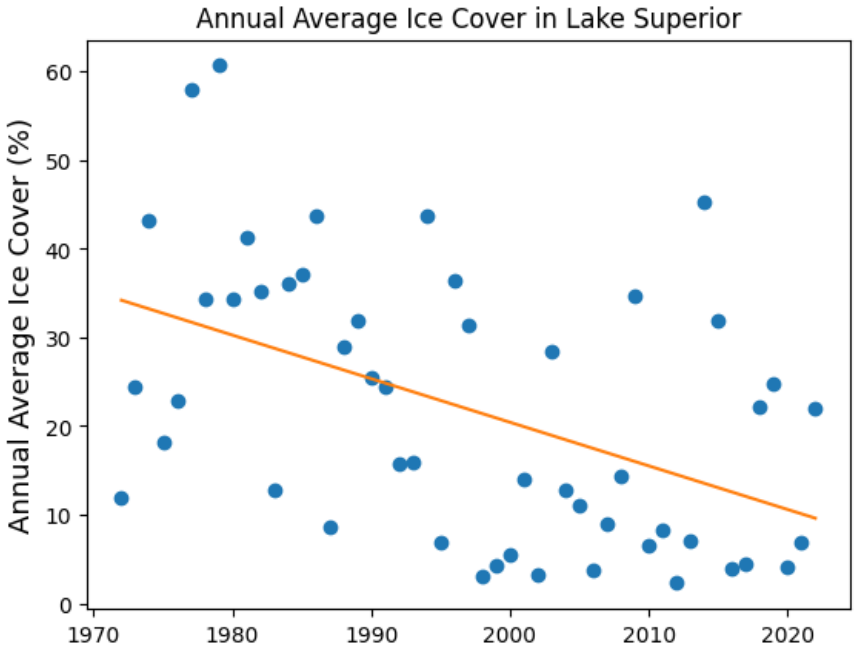

Figure 4.8: Annual average ice cover in Lake Superior; 1971-2022.

Figure 4.9 shows the relationship between summer stratification and annual average lake ice cover. The correlation isn't significantly strong (r=0.44, p-value=0.005), but the trend doesn't exactly appear linear.

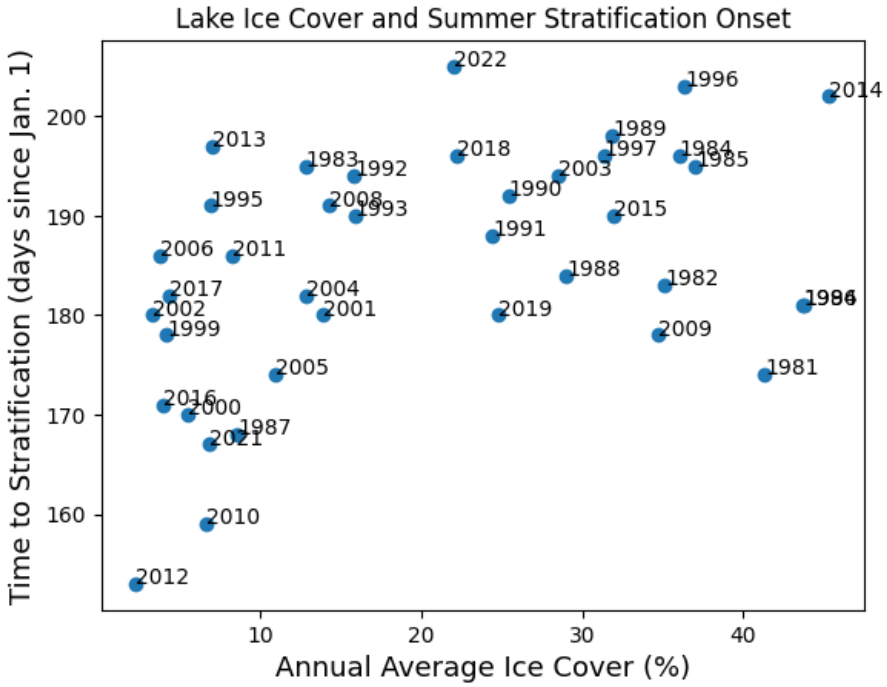

Figure 4.9: Onset of summer stratification as a function of annual average ice cover.

The initial large spread of dates at low ice percentage is a clear statement that stratification onset is not primarily dependent on ice cover, at least not when using annual averages.

A more accurate representation of the yearly effects of ice cover on lake heating is the annual total amount of shortwave energy deflected due to ice, $Q_{SW,out}$. We compute $Q_{SW,out}$ according to Eq.2.12, using daily average ice cover values and then summing. Initially, the albedo constant a_{ice} is set to 0.7. Figure 4.10 displays this trend, which appears to be decreasing over time, aside from the outlying datapoint of 2014's extreme winter at 1.2 GJ.

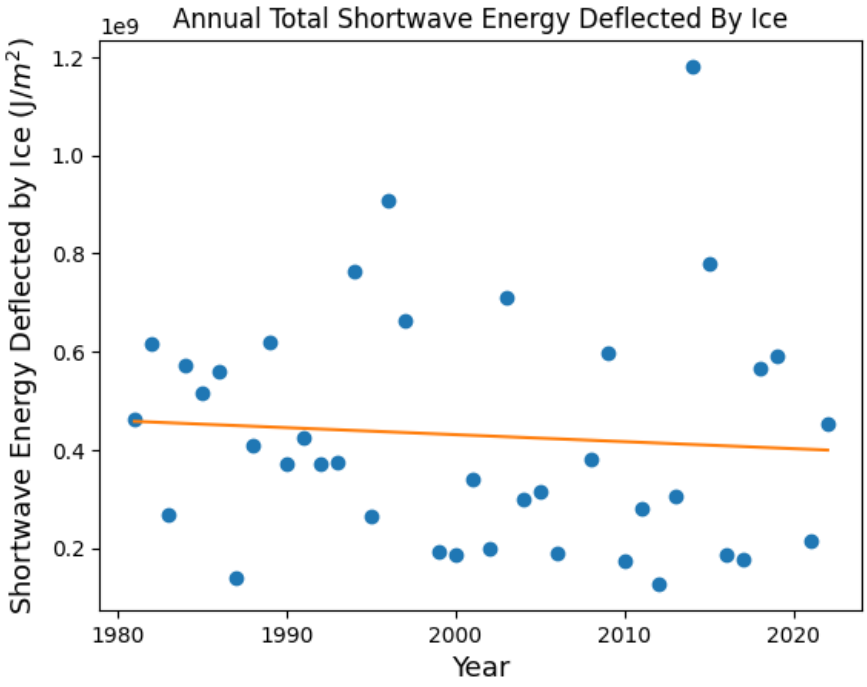

Figure 4.10: Annual total of deflected shortwave radiation due to ice's albedo, calculated from daily averages of Lake Superior ice cover.

The onset of summer stratification as a function of annual total deflected shortwave energy is plotted in Figure 4.11. Once again, the initial portion of this graph shows a large spread of values, which is now more consistently clumped. Evaluating the linearity between these factors results in a stronger correlation (r=0.58, p=0.0001) than that of stratification and annual average ice cover. It's possible that the relationship is only linear after a certain amount of shortwave is deflected from ice cover - it appears that the linear fit best includes values after about 0.2 GJ/m^2.

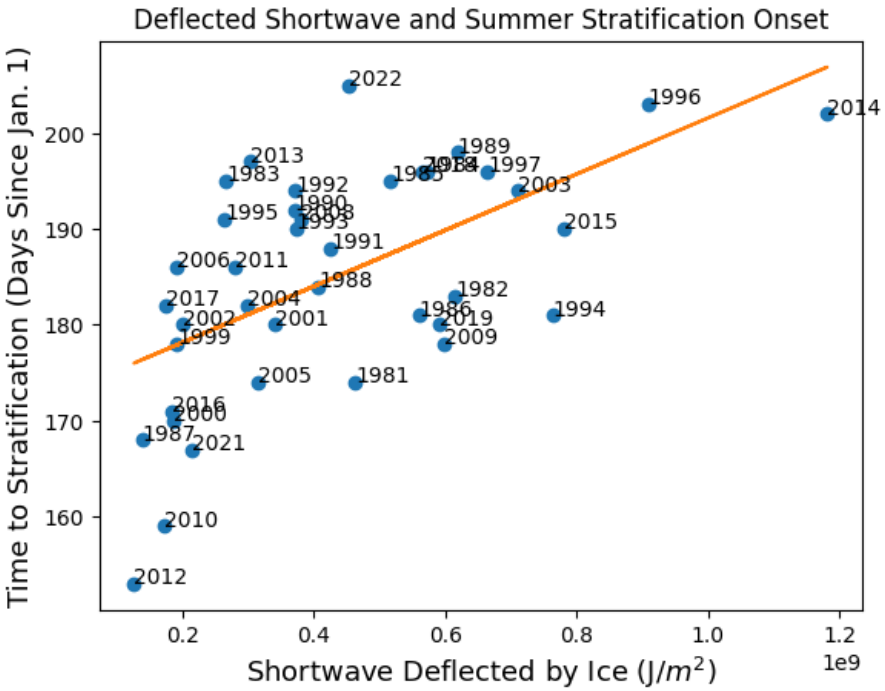

Figure 4.11: Onset of summer stratification as a function of ice-deflected shortwave radiation in Lake Superior.

As before, we can obtain an estimate for heat flux from this graph. Following the conversion process listed previously gives a net shortwave heat flux value of 395 W/m^2. The slope is positive but this value represents negative flux, as we are evaluating deflected energy. This value is quite large, some of which may be a result of overestimating the albedo constant at $\alpha_{ice} = 0.7$. Recomputing the slope using a more realistic albedo constant of 0.5 results in an outgoing flux value of 274 W/m^2. This represents that each day of delay in stratification corresponds to an extra 274 W/m^2 of outgoing shortwave radiation.

This value is still suspiciously large on a few measures. Firstly, it's more than the typical amount of incoming shortwave radiation on a given day during the ice-covered season (150-200 W/m^2). It is also significantly more than the range

of annual average outgoing shortwave radiation (10-70 W/m^2), shown in Figure 4.12.

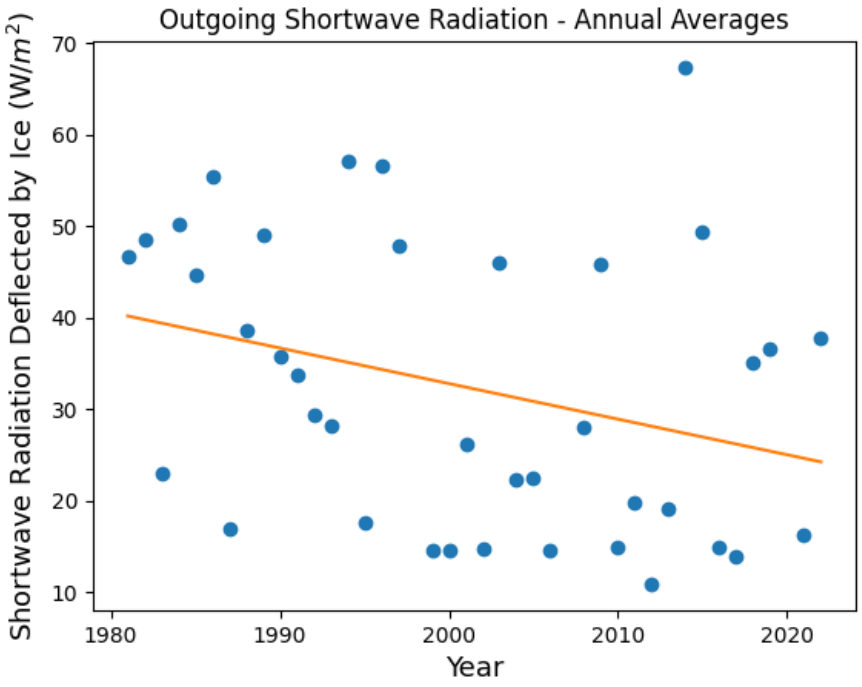

Figure 4.12: Annual averages of outgoing shortwave radiation due to the presence of ice.

Lastly, this estimate is more than the total net heat flux given from the fit of summer stratification vs. winter heat content (-243 W/m^2). Referring back to Figure 2.4, all surface flux terms are negative in the winter, therefore the shortwave flux prediction of -274 W/m^2 is not possible.

While annual averages aren't the best representation, Figure 4.12 shows many years with a significant portion of shortwave deflected due to ice cover.

Given the information from these plots and related calculations/comparisons, ice is not a great standalone predictor of stratification date, but it may still impact the timing indirectly through its effects on heat content, which will next be

explored.

First, we show the correlation between winter heat content and ice cover in Figure 4.13. These factors are both functions of winter air temperature, so it is unsurprising that they have a strong, negatively linear association (r=-0.82, p=0.0003) - colder winters with less total heat content tend to experience greater ice cover, and warmer years correspond with less ice.

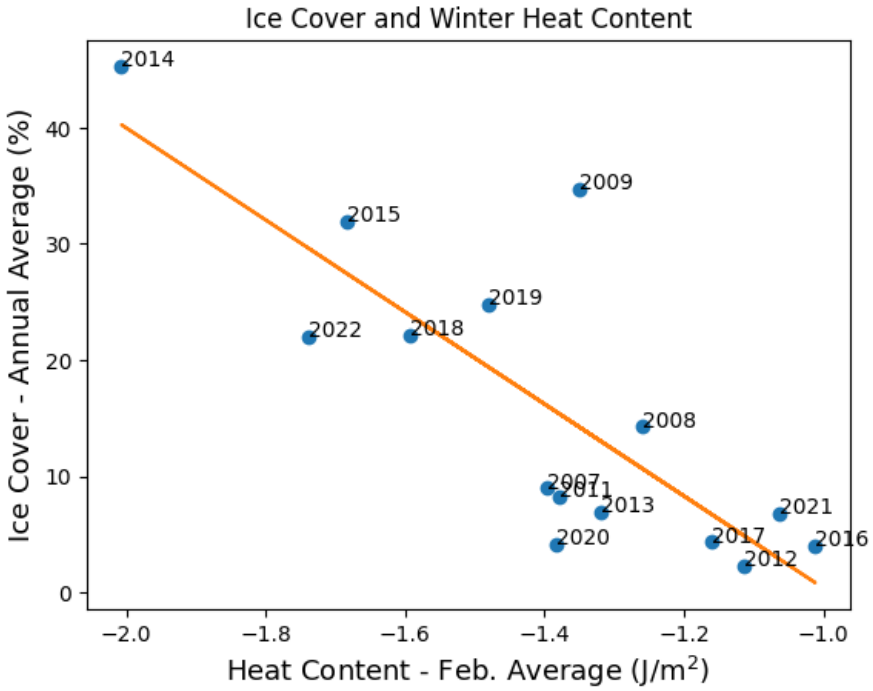

Figure 4.13: Correlation between annual average ice cover and winter average heat content.

There are a few clues that may help determine whether there is a causal influence of ice cover on heat content.

A plot of monthly ice cover averages in Figure 4.14 shows February and March as the months of maximal ice cover. They share very similar mean values of 38.8 and 39.4, respectively, so correlations of February/March average heat content

should have a correlation just as strong as when only February is used, if ice is an influence. However, when changing to February/March, the correlation's strength goes down significantly to r=-0.63/p=0.01.

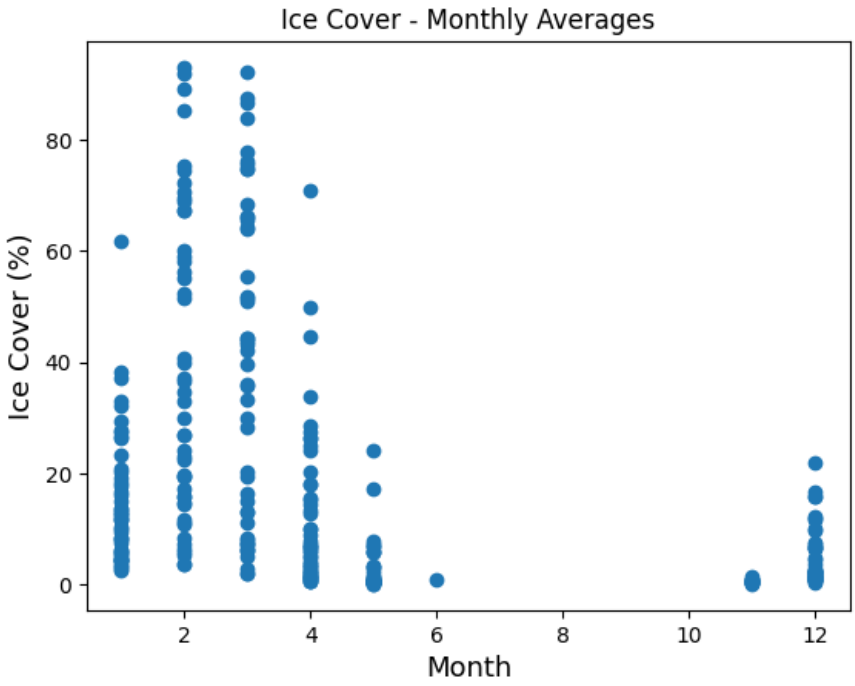

Figure 4.14: Monthly averages of total lake ice cover computer across data from 1972-2022.

This matches patterns of the relationship between winter heat content and air temperature, which also shows a stronger correlation when using just February vs. February/March. This may suggest that the association between heat content and ice cover is simply from their mutual dependence on air temperature, but more data is needed. Use of earlier periods to represent heat content (November, December) do not display a significant correlation with ice cover, hinting that heat content doesn't have a significant causal influence on ice cover either.

As mentioned in the introduction, it has been hypothesized that opposing

effects from ice could be cancelling out - ice prevents the absorption of sunlight, yet also traps already-accumulated heat that may otherwise be lost to the atmosphere. These effects can be examined by comparing heat content patterns in different regions of the lake. Like stratification, the formation of ice cover in Lake Superior is not uniform; it is affected by average depth and bathymetry of the regions, which are distinct (see Figure 3.5). Ice typically forms first in the Western region, followed by Central and then Eastern (Titze and Austin, 2014).

Heat content was first compared across these three regions by Titze and Austin (2014) for the high-ice winter season of 2009; they concluded that this year's excess ice cover resulted in a warmer spring, particularly in the Western, region due to insulation effects. These results are reproduced in Figure 4.15; daily averages of fractional lake ice cover and heat content at the Western mooring during the winter of 2009 are shown in alignment on the left, next to a plot of heat content cycles at the 3 mooring sites (WM, CM, and EM) from fall 2008-spring 2009 on the right.

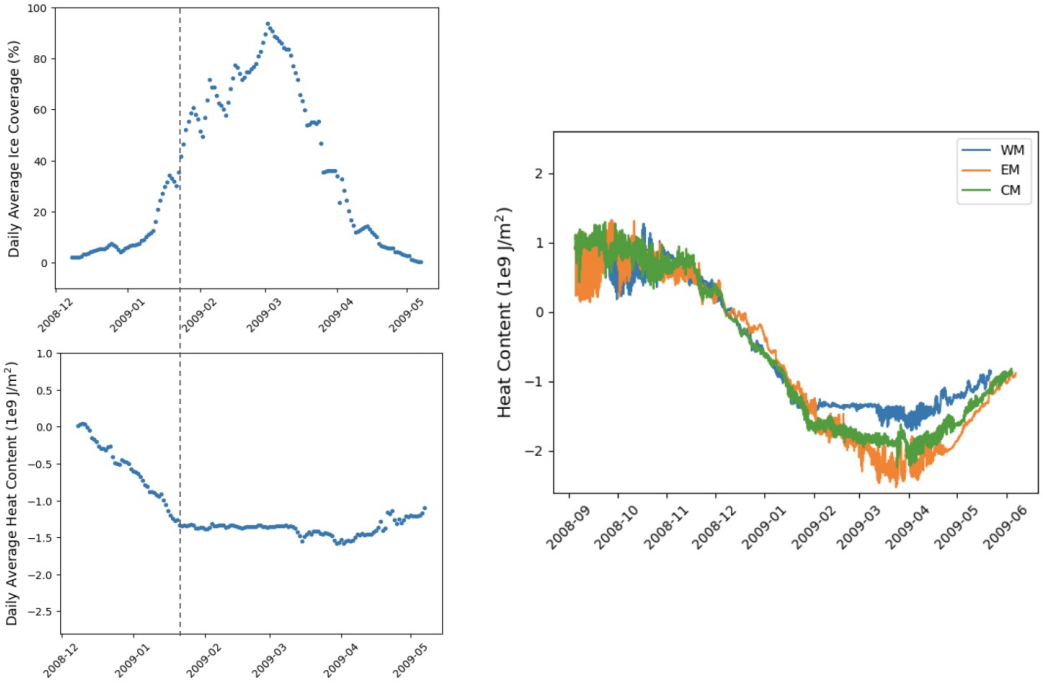

Figure 4.15: Left: Daily average total lake ice cover (top) and WM heat content (bottom); winter 2009. Dashed line marks the halt of heat transfer due to increasing formation of ice. Right: heat content cycles of the Fall 2008 deployment for all three regions.

Flattening of the WM heat content curve can be seen at about 40% ice cover. In the other regions it continues to decrease slightly at CM, and at EM it appears unaffected. Heat flux remains stagnant for the rest of the season in the Western region, leaving it off to a warmer start upon spring icemelt compared to the other areas.

Whether the insulation effect or the albedo effect dominates in a given winter season was hypothesized by Titze and Austin (2014) to be determined by the timing of ice formation, with further analysis from other high-ice years needed to confirm this. By now, we have data from two other years of significant ice cover; 2014 and 2015. Figures 4.16 and 4.17 show plots in similar fashion to the previous

for these years.

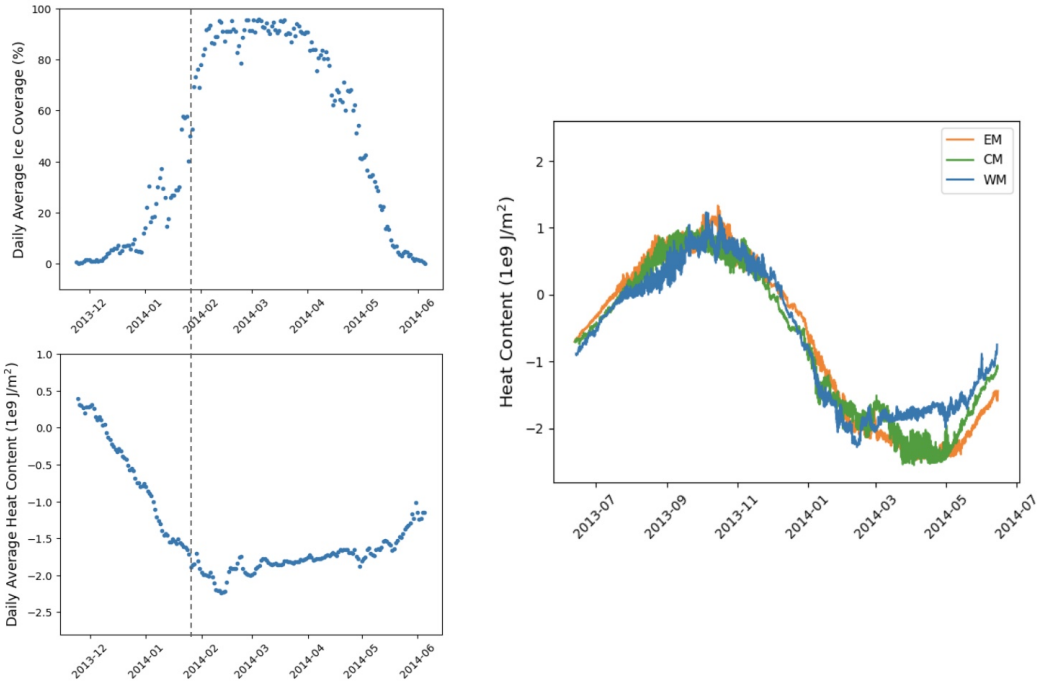

Figure 4.16: Left: Daily average total lake ice cover (top) and WM heat content (bottom); winter 2014. Right: heat content cycles of the Spring 2013 deployment for all three regions.

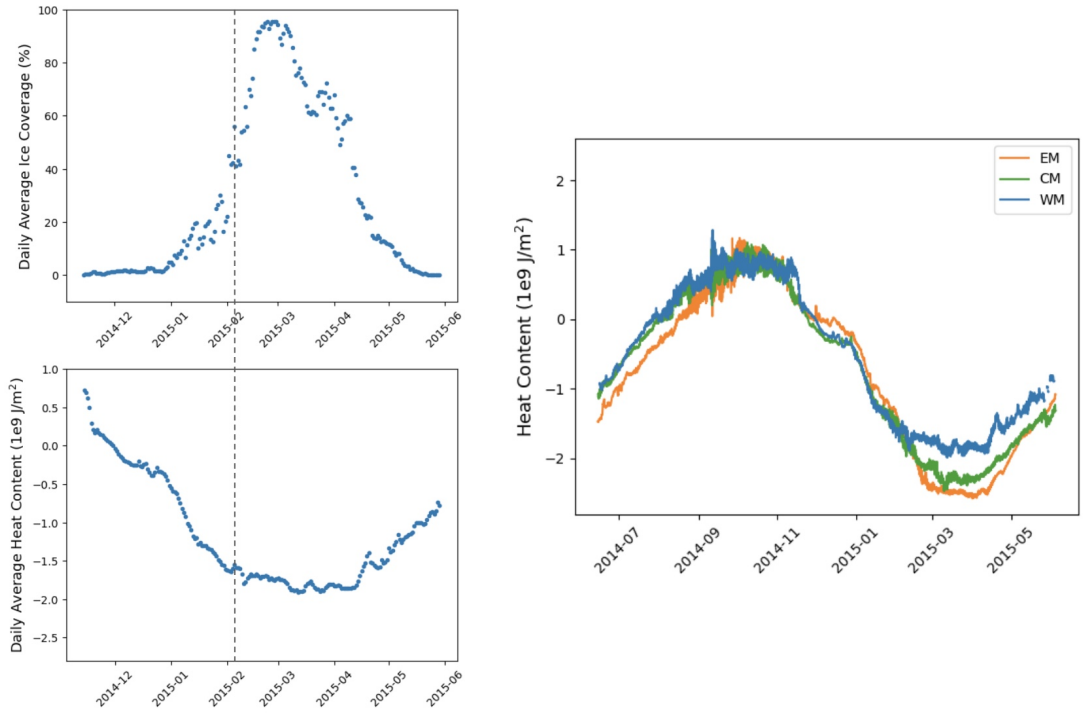

Figure 4.17: Left: Daily average total lake ice cover (top) and WM heat content (bottom); winter 2015. Right: heat content cycles of the Fall 2014 deployment for all three regions.

A pattern emerges from these three years of data - once ice cover reaches about 40%, heat flux essentially ceases at the Western region, slows considerably at CM, and is mostly unchanged at EM - though the loss of heat at EM in the winter of 2014 (year of maximal ice cover) slows more than other years, appearing even slightly warmer than CM by May. After ice melts past the 40% mark, heat content begins to increase across the lake.

The timing of ice formation consistently occurs around February, but duration of (high) ice cover varies. In 2009 and 2015, ice cover remains above the 40% mark for about 2 months, reaching 100% coverage for a few days in 2009 and a few weeks in 2015. In 2014, there are almost 4 months of high ice cover, with 2 of

those months at 100% coverage. Any resulting differences in heat content patterns aren't immediately obvious; heat content data across the lake during other high-ice years where ice forms earlier or later in the season would help address the question of timing-based effects of ice cover.

An interesting characteristic is the correspondence of mid-winter ice loss with short but dramatic dips in heat content, observed in 2014 during mid-February and to a lesser degree in mid-March of 2009 and 2015. Lacking the insulation from ice cover, colder air temperatures result in heat loss from the lake. But that isn't the end of the story; immediately after the initial heat loss, there is a slight increase observed in all three of these years even when ice re-forms, which is likely due to absorbed shortwave radiation during the temporary ice decline. It appears that these two behaviors cancel out, as heat content returns to levels prior to ice loss. It then remains constant once again until spring icemelt.

Overall it seems that the presence of significant ice cover has a noticeable insulating effect on heat content in the shallower Western region, where minimal values that would have been reached without insulation from ice cover are not reached. This is further demonstrated by comparing patterns of the low-ice winter of 2011 - daily average ice cover was around 10%-20%, never reaching beyond 40%. As a result, the outward flow of heat is unimpeded by ice cover and heat content remains consistent between the three regions, as shown in Figure 4.18.

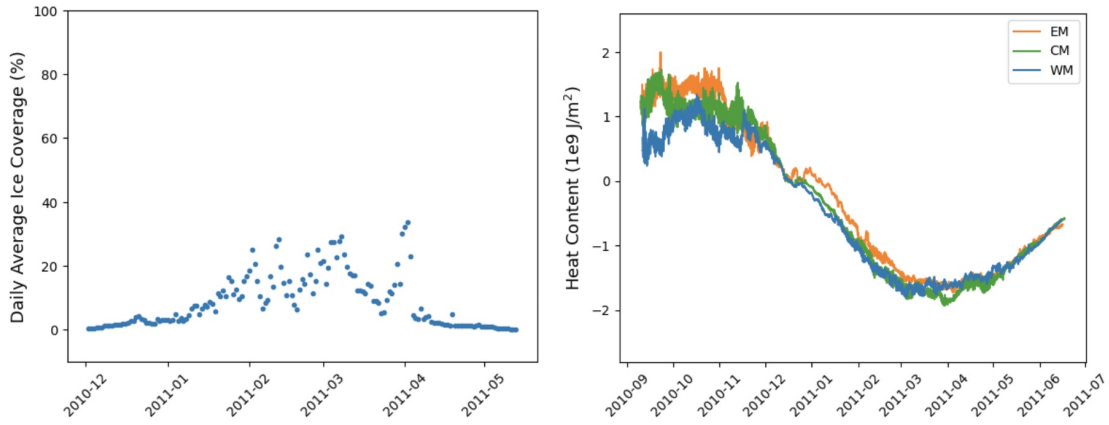

Figure 4.18: Winter '11 daily average ice cover and heat content cycles from the Fall 2010 deployment for all three regions.

Even in high-ice years, heat content values across the lake more or less converge upon the summer transition, but the Western region does tend to be warmer in the earlier part of the season as a result of insulation. This can lead to earlier stratification at this location - stratification at WM took place 2 weeks earlier than the other regions in 2009. This is important to consider, as most of our data is from the Western region.

Taking one last look at the winter season of 2009, it is a noticeable outlier in a few ways - in Figure 4.9, we see that it stratifies earlier than all of the other years with greater than 30% annual average ice cover except 1981. In Figure 4.12, it has greater winter heat content than many other years with this much, and sometimes less, ice cover. It remains somewhat of a mystery that the insulation effect was so strong in this season, which may be a result of other factors such as ice thickness or density that aren't reflected in this data.

Despite the complex effects of ice cover, related differences in heat content appear small compared to variations across the years. It remains true that years with high-ice cover are correlated with less winter heat content and later stratification

date, all of which are principally influenced by winter seasonal air temperature.

4.3 Air Temperature

We begin by showing the relationship between winter seasonal air temperature and summer stratification as well as summer SWTs in Figure 4.19. The correlations are significant (AT/stratification: r=0.69, p=4e-6; AT/SWTs: r=0.64, p=2e-7).

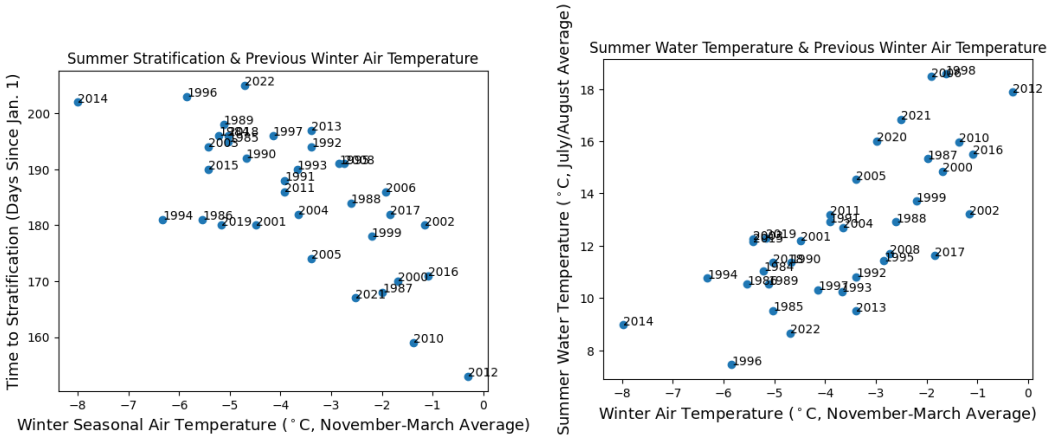

Figure 4.19: Left: Summer stratification onset vs. winter seasonal air temperature (November-March average). Right: Summer average SWT (July/August) vs. winter seasonal air temperature.

The association between winter air temperatures and following summer average heat content is of similar strength (r=0.64, p=0.007), though the p-value is a bit larger and the plot doesn't show as tight of a linear fit as those of Figure 4.19. The correlation between summer seasonal air temperature and following winter heat content is insignificant (r=0.13, p=0.6). These plots are shown in Figure 4.20. The same lack of influence is suspected between summer air temperatures and following winter water temperatures/stratification, though we lack the relevant SWT data to show this.

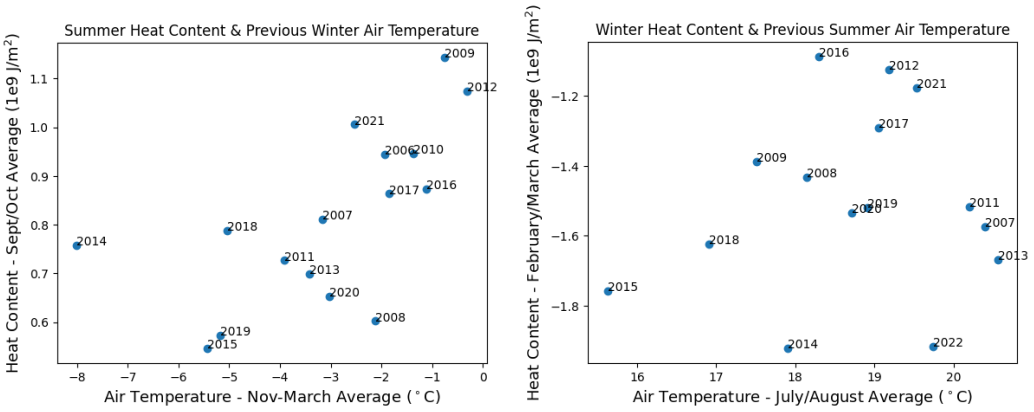

Figure 4.20: a. Left: Summer (September/October) average heat content and previous winter air temperature (November-March). b. Right: Winter (February/March) average heat content and previous summer air temperature (July/August).

Winter seasonal air temperature has the strongest relationship with winter heat content (r=0.84, p-value=9e-05), as shown in Figure 4.21 (left). On the right in Figure 4.21 is the correlation between summer average heat content and summer seasonal air temperature (r=0.14, p=0.6), which is much weaker.

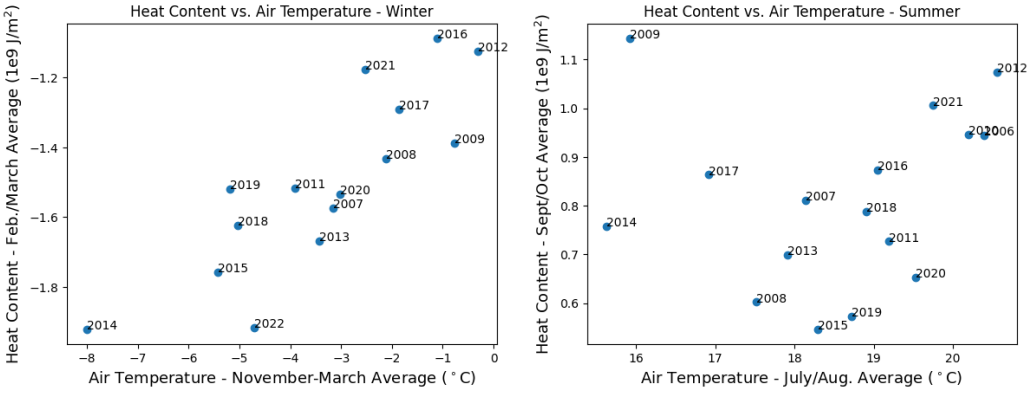

Figure 4.21: Left: Winter (February/March) average heat content as a function of winter seasonal air temperature. Right: Summer (September/October) average heat content as a function of summer seasonal air temperature.

Ice cover also exhibits a strong connection with winter air temperature (r=-0.78, p=6e-09), as shown in Figure 4.22.

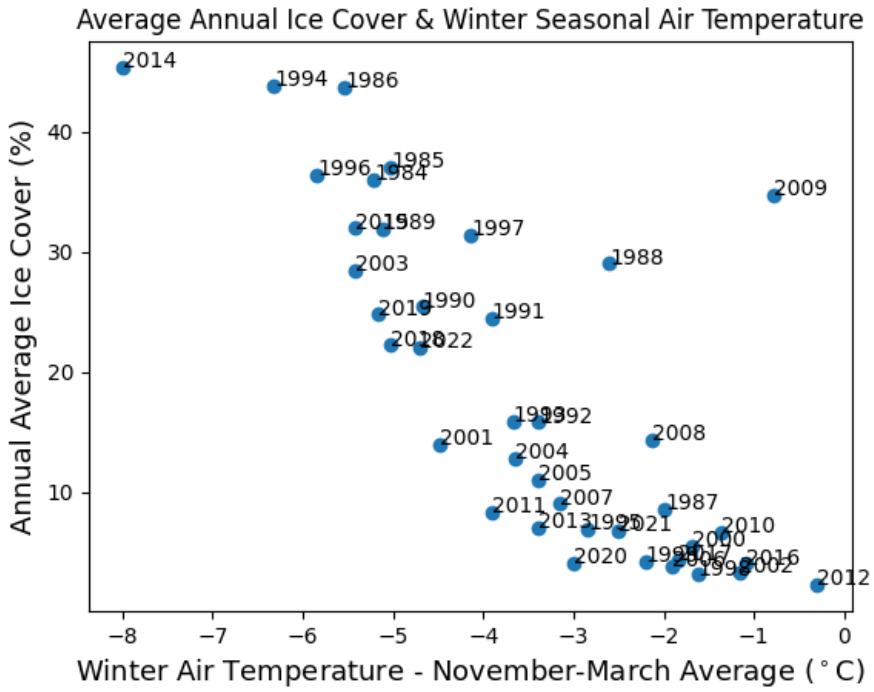

Figure 4.22: Annual average fractional lake ice cover as a function of winter seasonal air temperature.

While the fit parameters demonstrate a solid (anti)linearity, the form of this relationship appears distinctly curved, possibly indicating another nonlinear relationship with ice cover. 2009 remains even more of a mystery - despite some of the warmest winter seasonal air temperatures, the amount of ice cover is among the largest.

It is reasonable to say that winter heat content is dependent on air temperature, as the time period evaluated for air temperature is November to March where heat content is evaluated for February/March. Even removing data from the month of March, the connection is just as strong. The same can be said for

ice cover, as the highest percentages of ice cover are typically in February/March.

There is a significant seasonal difference in strength of air temperature's influence on heat content, which is again thought to be due to the difference in thermal structure of the lake between seasons. Another contribution to the contrasting seasonal variation of heat content (also previously attributed to thermal structure) arises when considering monthly average air temperatures over the years.

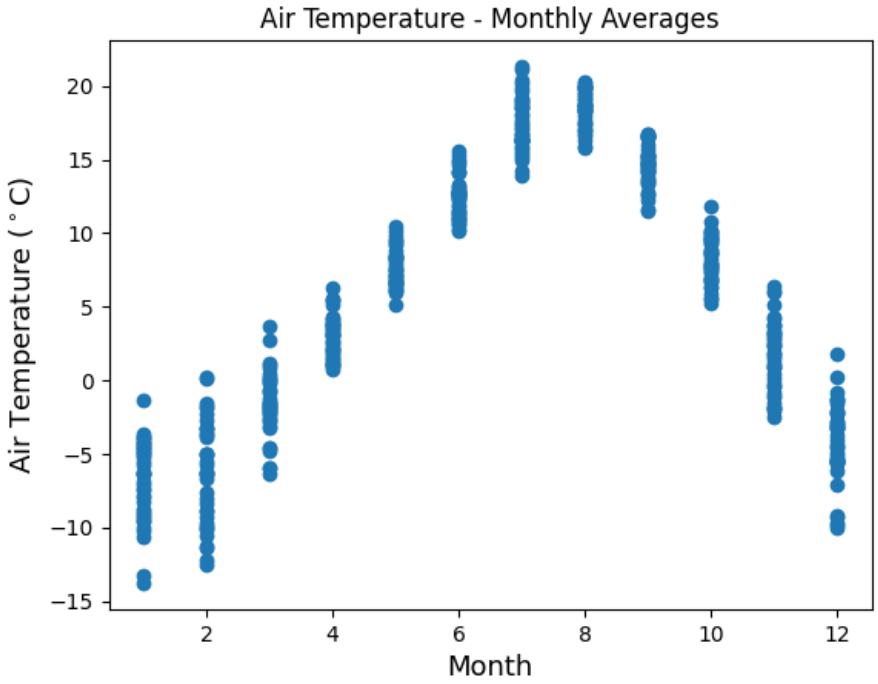

Figure 4.23: The annual cycle of monthly average air temperature, calculated from each year's hourly DISW3 data between 1983-2024.

As shown in Figure 4.23, the winter months have a much larger range in average air temperature than summer months. Accounting for the lag between water and air temperatures, the monthly variations line up well with monthly heat content variations seen in Figure 4.2. This solidifies the dependence of winter heat content on air temperature.

Figure 4.24 shows another similarity between air temperature and heat content - the somewhat surprising lack of a defined trend in either winter or summer seasonal averages.

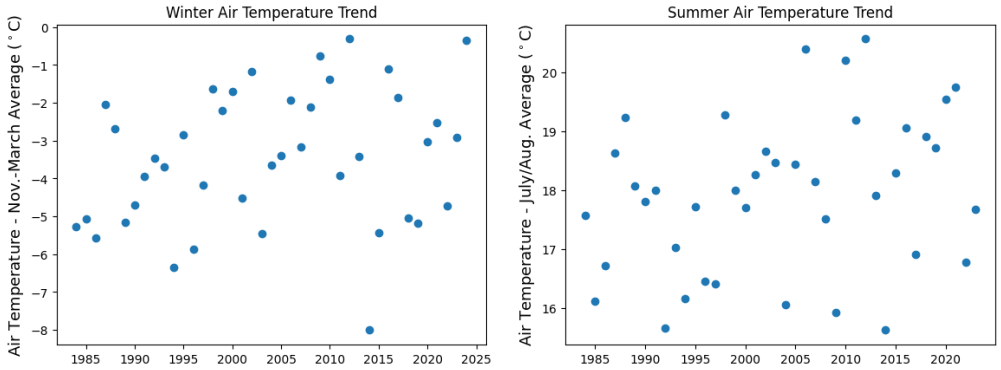

Figure 4.24: Winter (left) and summer (right) seasonal air temperatures for each year.

Linear fits of these trends are weak ($r<0.3$, $p>0.05$). It is again apparent that more data is necessary to determine whether a pattern is evolving.

The last and perhaps most surprising find is the connection between winter heat content and *following* summer air temperatures, which has a correlation of 0.53 and a p-value of 0.04. This is plotted in Figure 4.25.

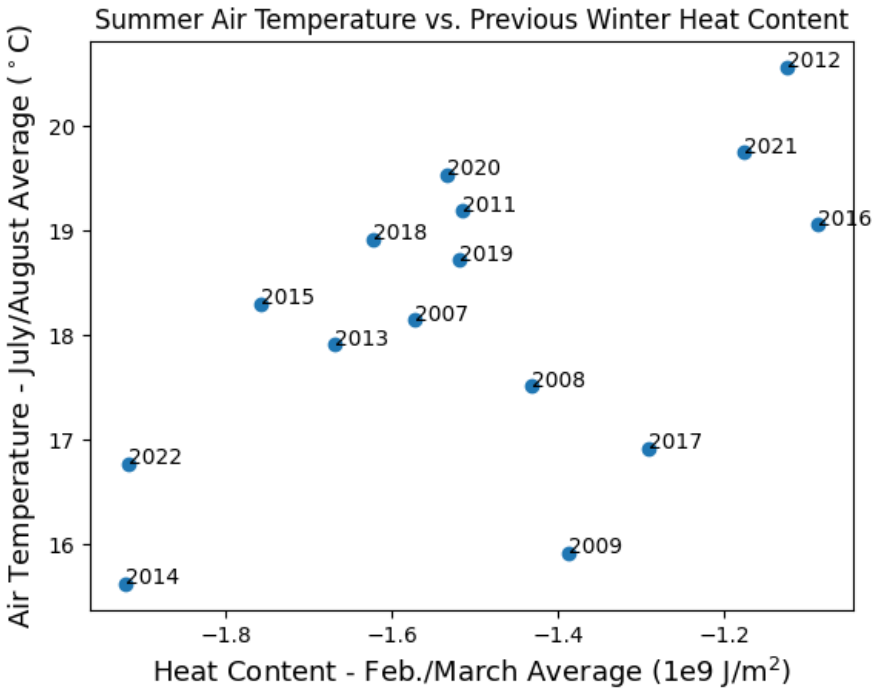

Figure 4.25: Summer air temperatures (July/August average) as a function of previous winter heat content (February/March average).

The connection between heat content and surface air temperature was previously established for the Arctic Ocean by Serreze and Francis (2006), and was attributed to the loss of sea ice. It is unexpected that this effect would be present in a much smaller body of water that experiences considerably shorter periods of ice cover. Further analysis adds evidence that ice cover may play an appreciable role; the correlation between ice cover and summer air temperatures is even slightly stronger (r=-0.6, p=7e-5) than heat content and air temperatures. Whether this is simply a result of having more ice cover than SSWT data remains to be seen.

Summer air temperature as a function of the previous winter's ice cover is shown in Figure 4.26 on the left. Summer and previous winter air temperatures are shown on the right in Figure 4.26; this correlation is moderate (r=0.49,

p=0.002), leaving us to conclude that winter air temperatures influence summer air temperatures through effects on other lake heating mechanisms such as heat content and ice cover.

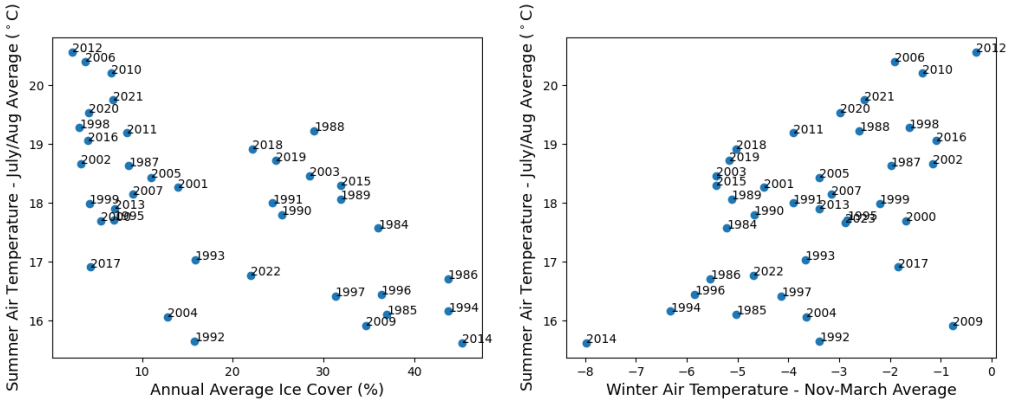

Figure 4.26: Summer air temperatures (July/August average) as a function of previous winter ice cover (annual average) on the left, and winter seasonal air temperatures (November-March average) on the right.

Summer air temperatures have no such effect on the following winter; the correlation is essentially nonexistent (r=0.1, p=0.55).

The effect these winter factors have on summer air temperatures is impressive. However, this analysis is restricted to air temperature data taken at Devil's Island, which is in the middle of Lake Superior. It remains to be seen whether air temperatures of the surrounding land are affected in similar ways. These effects don't appear to extend past the summer season, but this connection serves to demonstrate the power of winter conditions on summer heating trends both in and around the lake.

Chapter 5

Conclusion

Heat content is the most inclusive and indicative measure of a lake's heating response. For the first time, we have effectively demonstrated that winter heat content is a key predictor of summer stratification in Lake Superior, outweighing both ice cover and air temperature. These factors are strongly interconnected, with winter air temperature identified as the prime influence of winter lake thermal conditions through its effects on water temperature and ice cover formation. Together, these characteristics impact the timing of summer stratification and the extent of the following rise in surface water temperatures.

We have shown the annual cycle of heat content across 23 deployments between 2006-2022; the shape is consistent from year to year, generally reaching a low around February-March and a high in September/October. Variations in winter heat content are larger than in the summer, which is thought to be a result of the larger variation in winter air temperature as well as seasonal differences in thermal structure. Heat flux during the winter-to-summer seasonal transition remains constant, which allows for reliable predictions of the timing of summer

stratification from winter heat content measurements. Among the various relationships examined here, the strongest ones are: the onset of summer stratification and previous winter heat content, winter heat content and seasonal air temperatures, and winter heat content and ice cover. Winter heat content is the common link, which is a measure of its representative power as opposed to its influence.

It is also shown that heat content has a memory of about half of a year, which is seasonally dependent - the connection is much stronger between winter and subsequent summer heat content than between summer and following winter. This seasonal contrast continues to display itself in other areas - for example, while winter air temperature is the most important influencing factor of all, summer air temperatures have essentially no connection with conditions in following seasons. Much of this distinction is again attributed to differences in thermal structure of the water column between winter and summer; the summer surface layer (where all incoming heat is absorbed and stored) is much more shallow than in the winter, minimizing differences in heat content and allowing for swift heat loss in the fall mixing season. This essentially acts as a seasonal reset of heat content.

There are no definitive trends found in seasonal air temperature or heat content over the years, but there is an established decline in ice cover at about -.49+/-0.13%/year, matching previous literature values. Most of the notable associations presented are linear, matching our hypotheses based on Eqs. 2.18 and 2.19. One relationship that did not exhibit linearity was that of summer stratification and annual average ice cover, though plotting stratification as a function of deflected sunlight (due to ice's albedo) shows possible linearity after a certain amount of sunlight is deflected. Though ice cover is not a good predictor of stratification date, it can deflect a large amount of incoming sunlight, and likely has some indirect influence on the timing through its effects on surface heating. However,

the degree of ice's influence on lake heating is difficult to quantify, in part due to the opposing forces of its deflective and insulatory properties. Even from analysis of winter heat content, it proves difficult to separate the effects of ice cover, since winter heat content and ice cover are both functions of winter air temperature. Comparing correlations between ice cover and heat content seems to indicate a lack of causal influence in either direction, though this may be due to a lack of data. There is contradicting evidence that the effects of ice cover may be responsible for an identified relationship between summer air temperatures and winter heat content, but further analysis is needed.

Taking into account the effects of ice cover in the form of predicted outgoing shortwave radiation (10-70 W/m^2), our estimated total net heat flux of -243 W/m^2 is reasonably close to Lofgren & Zhu's (1999) ice-free February estimate of -189 W/m^2, but is pretty far from their March estimate of -18 W/m^2. This study used a single year of data from the 1990's and did not take into account ice cover, so it is not an ideal comparison, but the relative closeness of values is promising.

While the exact effects related to ice's deflective properties on stratification remain unclear, subregional comparisons of heat content patterns offer insight regarding the effects of insulation. During years of high ice cover when there is at least 40% total lake ice coverage, it is seen that heat loss is impeded - particularly in the Western region - due to insulatory effects of ice. This contributes to earlier stratification of the area by up to two weeks, though effects on the lake as a whole are unknown. Despite the insulating potential of ice cover in large amounts, these years generally correspond with cold air temperatures and a resulting degree of lake cooling that outweighs the effects of insulation.

The findings presented in this study are limited by the relatively small SSWT

dataset and a lack of data from years with high ice cover. Ice cover data does not include density or thickness information, which influence ice's albedo and insulation. Improvements could be made on the method of SSWT data interpolation and the method of determining stratification, but resulting differences are marginal. The Great Lakes have vast differences in size, depth, and latitude resulting in relatively unique seasonal behaviors both in and around the lakes. Caution should be applied when generalizing lake heating behaviors, which should be treated individually. Even the regions of Lake Superior exhibit differences in ice formation and surface warming; this provided the ability to analyze the effects of insulation from ice cover, which will be further aided with more years of data across the regions.

This study used estimations of shortwave radiation from a simplified equation that did not take into account cloud cover, which has been shown to be decreasing over time, leading to increasing amounts of sunlight reaching the Earth's surface (Anderson et al., 2021). Accounting for these factors could reveal significant effects on lake heating. Shortwave radiation was the only term of the four surface flux processes that was independently examined here; individual analysis of the other fluxes could add helpful insight. The longwave radiative term specifically is necessary to address the role of greenhouse gases in lake heating.

Winter surface water temperatures and consequently winter stratification was unexplored in this analysis. Although the NDBC surface buoys are not deployed for the November-April period, data from the first thermistors of subsurface moorings are adequate to analyze winter surface conditions due to the uniformity and depth of the surface layer during the winter season. Analyzing winter stratification and its influences will add significantly to our understanding of Lake Superior's yearly heating cycle.

Chapter 6

Bibliography

Anderson, E.J., Stow, C.A., Gronewold, A.D. et al. (2021). Seasonal overturn and stratification changes drive deep-water warming in one of Earth's largest lakes. Nat Commun 12, 1688. doi: 10.1038/s41467-021-21971-1.

Austin, J. A. and S. M. Colman (2007). Lake Superior summer water temperatures are increasing more rapidly than regional air temperatures: A positive ice-albedo feedback. Physical Research Letters, Vol. 34, L06604. doi: 10.1029/2006GL029021.

Austin, J. A. and S. M. Colman (2008). A century of temperature variability in Lake Superior. Limnology and Oceanography, 53. doi: 10.4319/lo.2008.53.6.2724.

Austin, J.A., E.B. Voytek, J. Halbur, and M.A. Macuiane (2011). Hands-on oceanography: Lake in a bottle—A laboratory demonstration of the unusual stability properties of freshwater. Oceanography, 24(4), 136–142.
doi: 10.5670/oceanog.2011.107.

Bennington, V., G. A. McKinley, N. Kimura, and C. H. Wu (2010). General circulation of Lake Superior: Mean, variability, and trends from 1979 to 2006. Journal of Geophysical Research, 115, C12015. doi: 10.1029/2010JC006261.

Bronselaer, B. and Zanna, L. (2020). Heat and carbon coupling reveals ocean warming due to circulation changes. Nature, 584, 227-233. doi: 10.1038/s41586-020-2573-5.

Church, J. A., N. J. White, L. F. Konikow, C. M. Domingues, J. G. Cogley, E. Rignot, J. M. Gregory, M. R. van den Broeke, A. J. Monaghan, and I. Velicogna (2011). Revisiting the Earth's sea-level and energy budgets from 1961 to 2008. Geophysical Research Letters, 38, L18601. doi: 10.1029/2011GL048794.

Cline, T., Bennington, V., Kitchell, J.F. (2013). Climate Change Expands the Spatial Extent and Duration of Preferred Thermal Habitat for Lake Superior Fishes. PLOS ONE, 8(4), e62279. doi: 10.1371/journal.pone.0062279

Cheng, L. J. and Coauthors (2023). Another year of record heat for the oceans. Advances in Atmospheric Sciences, 40, 963-974. doi: 10.1007/s00376-023-2385-2

Dijkstra, Henk (2008). "Dynamical Oceanography". Springer-Verlag, Berlin, Heidelberg.

Emanuel, Kerry A. (2013). Downscaling CMIP5 climate models show increased tropical cyclone activity over the 21st century. Proceedings of the National Academy of Sciences, 110 (30), 12219-12224. doi: 10.1073/pnas.13012931

Grannemann, N. and Reeves, H. (2005). "Great Lakes Basin Water Availability and Use". USGS National Assessment of Water Availability and Use in the Great Lakes Basin.

Environmental Protection Agency (2023). "Great Lakes Facts and Figures". https://epa.gov/greatlakes/great-lakes-facts-and-figures

Gronewold, A.D., Fortin, V., Lofgren, B., Clites, A., Stow, C.A., Quinn, F. (2013). Coasts, water levels, and climate change: A Great Lakes perspective. Climatic Change, 120, 697-711. doi: 10.1007/s10584-013-0840-2

Hutter, K., Wang, Y., Chubarenko, I.P. (2011). Phenomenological Coefficients

of Water. In: Physics of Lakes. Advances in Geophysical and Environmental Mechanics and Mathematics. Springer, Berlin, Heidelberg.
doi: 10.1007/978-3-642-15178-1_10

Krantzberg, G. and De Boer, C. (2008). A valuation of ecological services in the Laurentian Great Lakes Basin with an emphasis on Canada. American Water Works Association, 100, 100-111. doi: 10.1002/j.1551-8833.2008.tb09657.x

Lofgren, B.M., Zhu, Y. (1999). Seasonal climatology of surface energy fluxes on the Great Lakes. NOAA technical memorandum ERL GLERL, 112, GLERL contribution no. 1132.

Lofgren, B.M., Zhu, Y. (2000). Surface Energy Fluxes on the Great Lakes Based on Satellite-Observed Surface Temperatures 1992 to 1995. Journal of Great Lakes Research, 26(3), 305-314. doi: 10.1016/S0380-1330(00)70694-0

Matheson, D.H. and Munawar, M. (2009). Lake Superior Basin and its Development. Journal of Great Lakes Research, 4(3-4), 249-263. doi: 10.1016/S0380-1330(78)72196-9.

Mason, L. A., Riseng, C. M., Gronewold, A. D., Rutherford, E. S., Wang, J., Clites, A., ... & McIntyre, P. B. (2016). Fine-scale spatial variation in ice cover and surface temperature trends across the surface of the Laurentian Great Lakes. Climatic Change, 138, 71-83. doi: 10.1007/s10584-016-1721-2.

O'Reilly, C. M., Sharma, S., Gray, D. K., Hampton, S. E., Read, J. S., Rowley, R. J., ... & Zhang, G. (2015). Rapid and highly variable warming of lake surface waters around the globe. Geophysical Research Letters, 42(24), 10-773. doi: 10.1002/2015GL066235

Ozersky, T., Bramburger, A. J., Elgin, A. K., Vanderploeg, H. A., Wang, J., Austin, J. A., ... & Zastepa, A. (2021) The changing face of winter: lessons and questions from the Laurentian Great Lakes. Journal of Geophysical Research:

Biogeosciences, 126(6), e2021JG006247. doi: 10.1029/2021JG006247.

Schertzer, W.M. (1978). Energy Budget and Monthly Evaporation Estimates for Lake Superior. Journal of Great Lakes Research, 4(3-4), 320-330. ISSN 0380-1330. doi: 10.1016/S0380-1330(78)72201-X.

Schneider, P., S. J. Hook, R. G. Radocinski, G. K. Corlett, G. C. Hulley, S. G. Schladow, and T. E. Steissberg (2009). Satellite observations indicate rapid warming trend for lakes in California and Nevada. Geophysical Research Letters, 36, L22402. doi:10.1029/2009GL040846

Schneider, P. and Hook, S.J. (2010). Space observations of inland water bodies show rapid surface warming since 1985. Geophysical Research Letters, 37(22).

Serreze, M.C., Francis, J.A. (2006). The Arctic Amplification Debate. *Climatic Change* **76**, 241–264. doi: 10.1007/s10584-005-9017-y.

Titze, D. J., and Austin, J. A. (2014). Winter thermal structure of Lake Superior. Limnology and oceanography, 59(4), 1336-1348.
doi: 10.4319/lo.2014.59.4.1336.

Trumpickas, J., Shuter, B.J., Minns, C.K. (2009). Forecasting impacts of climate change on Great Lakes surface water temperatures. Journal of Great Lakes Research, 35(3), 454-463. doi: 10.1016/j.jglr.2009.04.005.

United States Naval Observatory (1978). *Almanac For Computers*. Nautical Almanac Office.

Wang, Y.J. and Wang, L.Y. (2011). Water chain encapsulated in carbon nanotube revealed by density functional theory. International Journal of Quantum Chemistry, 111: 4465-4471. doi: 10.1002/qua.22994.

Wikimedia user "Darekk2" (2015). *Lake Superior bathymetry map* [png]. `https://commons.wikimedia.org/wiki/File:Lake_Superior_bathymetry_map.png`

Xue, P., D. J. Schwab, and S. Hu. (2015). An investigation of the thermal

response to meteorological forcing in a hydrodynamic model of Lake Superior. Journal of Geophysical Research: Oceans, 120, 5233–5253.
doi: 10.1002/2015JC010740.

Yang, B., Wells, M. G., McMeans, B. C., Dugan, H. A., Rusak, J. A., Weyhenmeyer, G. A., ... & Young, J. D. (2021). A new thermal categorization of ice-covered lakes. Geophysical Research Letters, 48(3). doi: 10.1029/2020GL091374

Zhong, Y., Notaro, M., Vavrus, S. and Foster, M.J. (2016). Recent accelerated warming of the Laurentian Great Lakes: Physical Drivers. Limnology and Oceanography, 61(5), 1762-1786. doi: 10.1002/lno.10331

Appendix A

Acronyms

- AT: Air temperature
- EPA: Environmental Protection Agency
- GLERL: Great Lakes Environmental Research Laboratory
- LLO: Large Lakes Observatory
- NDBC: National Data Buoy Center
- NOAA: National Oceanic and Atmospheric Administration
- SWT: surface water temperature
- SSWT: subsurface water temperature

Appendix B

Graphs

B.1 Surface Water Temperature

Individual annual surface water temperature plots are shown below.

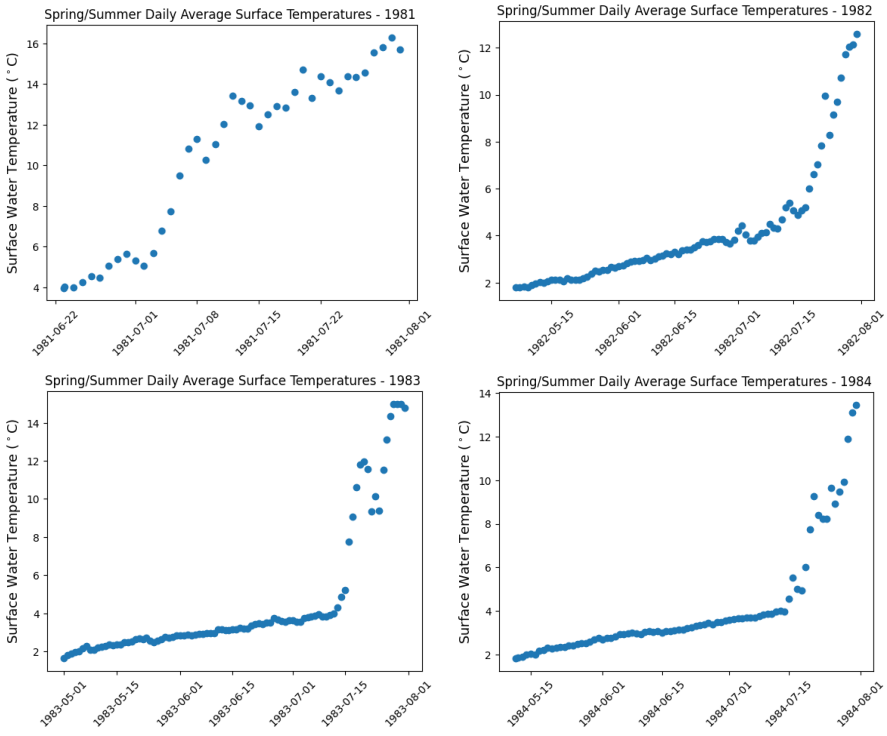

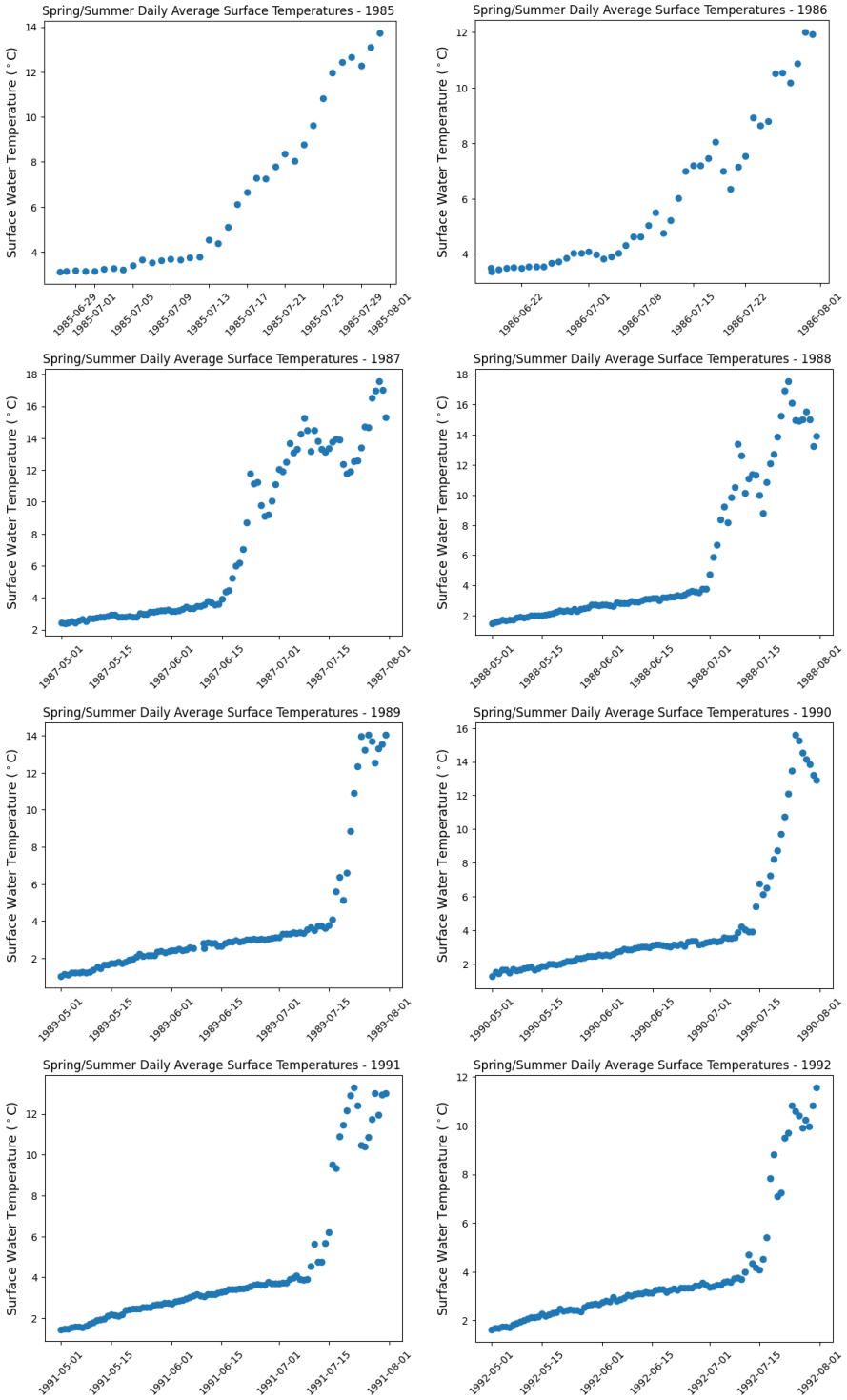
Spring/Summer Daily Average Surface Temperatures - 1985
Surface Water Temperature (°C)
Spring/Summer Daily Average Surface Temperatures - 1986
Surface Water Temperature (°C)
Spring/Summer Daily Average Surface Temperatures - 1987
Surface Water Temperature (°C)
Spring/Summer Daily Average Surface Temperatures - 1988
Surface Water Temperature (°C)
Spring/Summer Daily Average Surface Temperatures - 1989
Surface Water Temperature (°C)
Spring/Summer Daily Average Surface Temperatures - 1990
Surface Water Temperature (°C)
Spring/Summer Daily Average Surface Temperatures - 1991
Surface Water Temperature (°C)
Spring/Summer Daily Average Surface Temperatures - 1992
Surface Water Temperature (°C)

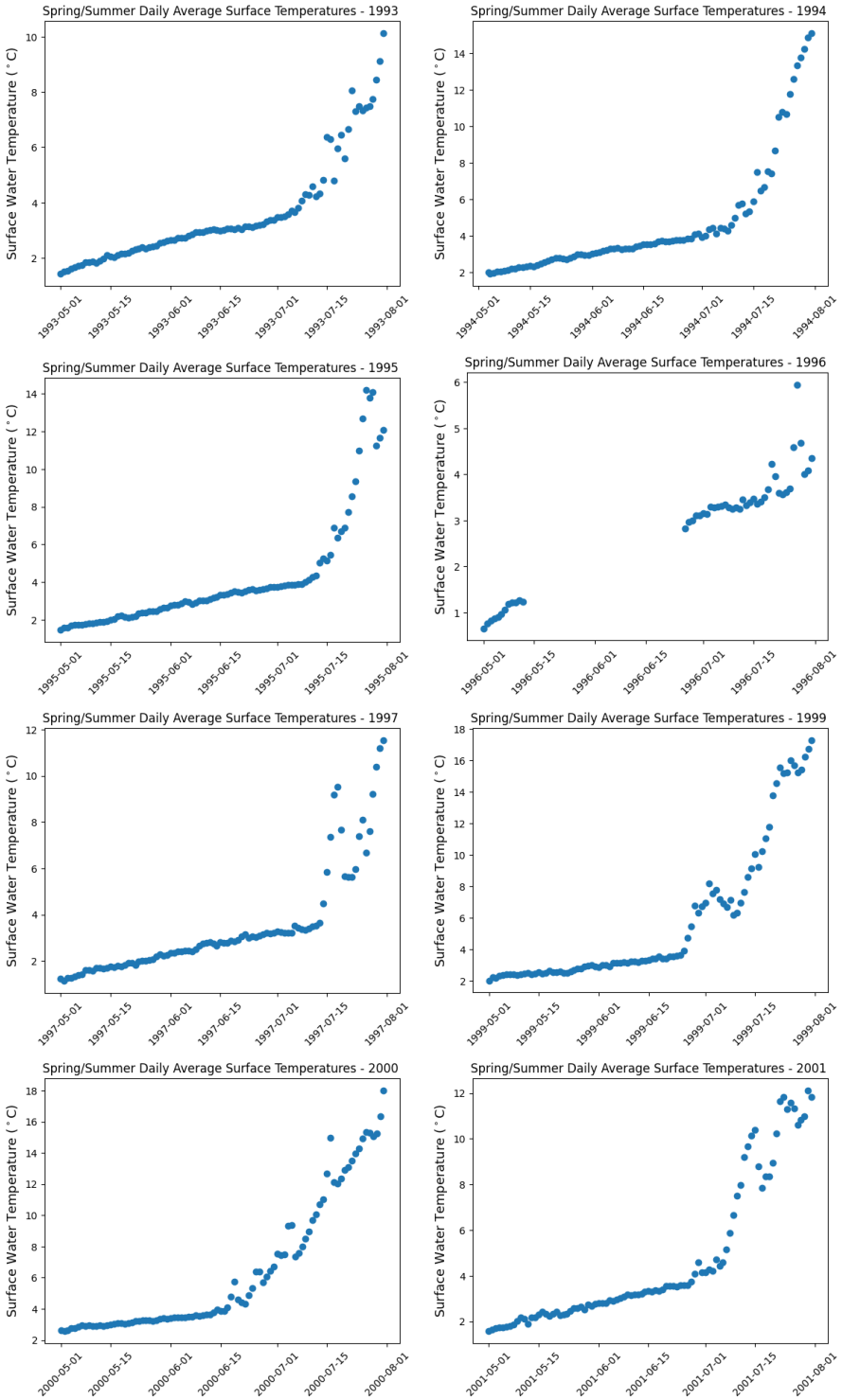
Spring/Summer Daily Average Surface Temperatures - 1993
Surface Water Temperature (°C)
Spring/Summer Daily Average Surface Temperatures - 1994
Surface Water Temperature (°C)
Spring/Summer Daily Average Surface Temperatures - 1995
Surface Water Temperature (°C)
Spring/Summer Daily Average Surface Temperatures - 1996
Surface Water Temperature (°C)
Spring/Summer Daily Average Surface Temperatures - 1997
Surface Water Temperature (°C)
Spring/Summer Daily Average Surface Temperatures - 1999
Surface Water Temperature (°C)
Spring/Summer Daily Average Surface Temperatures - 2000
Surface Water Temperature (°C)
Spring/Summer Daily Average Surface Temperatures - 2001
Surface Water Temperature (°C)

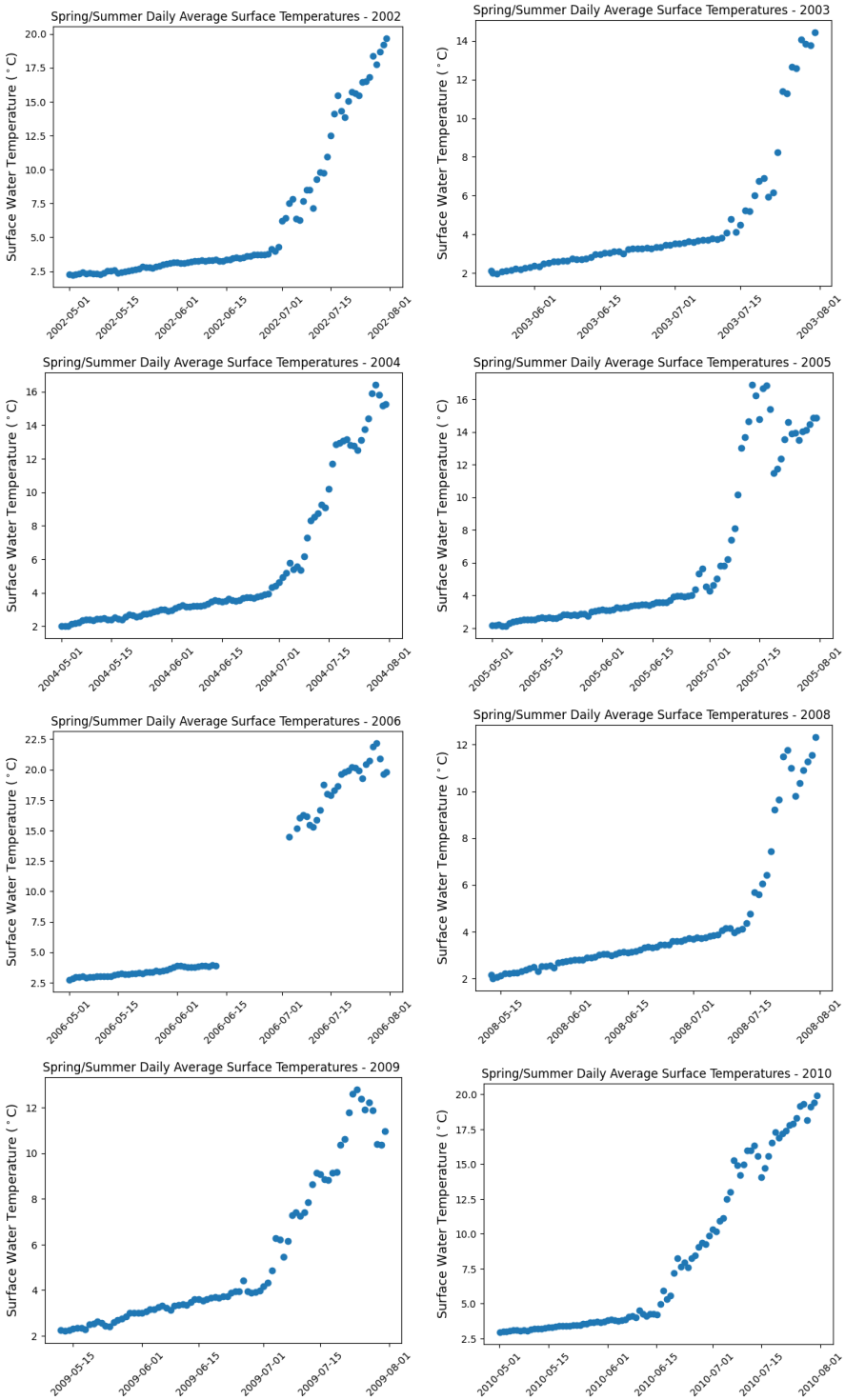
Spring/Summer Daily Average Surface Temperatures - 2002
Surface Water Temperature (°C)
2002-05-01
2002-05-15
2002-06-01
2002-06-15
2002-07-01
2002-07-15
2002-08-01
Spring/Summer Daily Average Surface Temperatures - 2003
Surface Water Temperature (°C)
2003-06-01
2003-06-15
2003-07-01
2003-07-15
2003-08-01
Spring/Summer Daily Average Surface Temperatures - 2004
Surface Water Temperature (°C)
2004-05-01
2004-05-15
2004-06-01
2004-06-15
2004-07-01
2004-07-15
2004-08-01
Spring/Summer Daily Average Surface Temperatures - 2005
Surface Water Temperature (°C)
2005-05-01
2005-05-15
2005-06-01
2005-06-15
2005-07-01
2005-07-15
2005-08-01
Spring/Summer Daily Average Surface Temperatures - 2006
Surface Water Temperature (°C)
2006-05-01
2006-05-15
2006-06-01
2006-06-15
2006-07-01
2006-07-15
2006-08-01
Spring/Summer Daily Average Surface Temperatures - 2008
Surface Water Temperature (°C)
2008-05-15
2008-06-01
2008-06-15
2008-07-01
2008-07-15
2008-08-01
Spring/Summer Daily Average Surface Temperatures - 2009
Surface Water Temperature (°C)
2009-05-15
2009-06-01
2009-06-15
2009-07-01
2009-07-15
2009-08-01
Spring/Summer Daily Average Surface Temperatures - 2010
Surface Water Temperature (°C)
2010-05-01
2010-05-15
2010-06-01
2010-06-15
2010-07-01
2010-07-15
2010-08-01

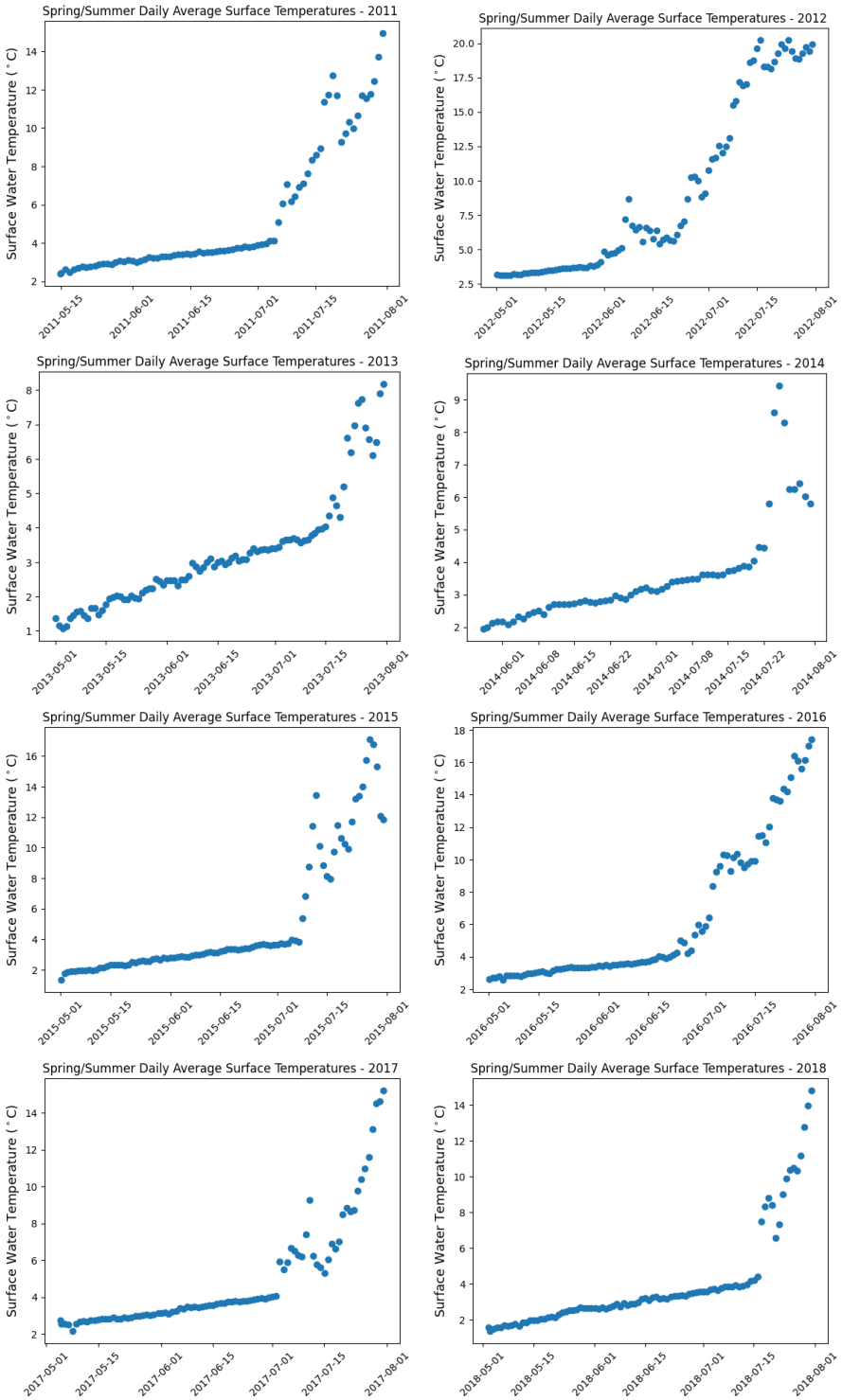
Spring/Summer Daily Average Surface Temperatures - 2011
Surface Water Temperature (° C)
2011-05-15
2011-06-01
2011-06-15
2011-07-01
2011-07-15
2011-08-01
Spring/Summer Daily Average Surface Temperatures - 2012
Surface Water Temperature (° C)
2012-05-01
2012-05-15
2012-06-01
2012-06-15
2012-07-01
2012-07-15
2012-08-01
Spring/Summer Daily Average Surface Temperatures - 2013
Surface Water Temperature (° C)
2013-05-01
2013-05-15
2013-06-01
2013-06-15
2013-07-01
2013-07-15
2013-08-01
Spring/Summer Daily Average Surface Temperatures - 2014
Surface Water Temperature (° C)
2014-06-01
2014-06-08
2014-06-15
2014-06-22
2014-07-01
2014-07-08
2014-07-15
2014-07-22
2014-08-01
Spring/Summer Daily Average Surface Temperatures - 2015
Surface Water Temperature (° C)
2015-05-01
2015-05-15
2015-06-01
2015-06-15
2015-07-01
2015-07-15
2015-08-01
Spring/Summer Daily Average Surface Temperatures - 2016
Surface Water Temperature (° C)
2016-05-01
2016-05-15
2016-06-01
2016-06-15
2016-07-01
2016-07-15
2016-08-01
Spring/Summer Daily Average Surface Temperatures - 2017
Surface Water Temperature (° C)
2017-05-01
2017-05-15
2017-06-01
2017-06-15
2017-07-01
2017-07-15
2017-08-01
Spring/Summer Daily Average Surface Temperatures - 2018
Surface Water Temperature (° C)
2018-05-01
2018-05-15
2018-06-01
2018-06-15
2018-07-01
2018-07-15
2018-08-01

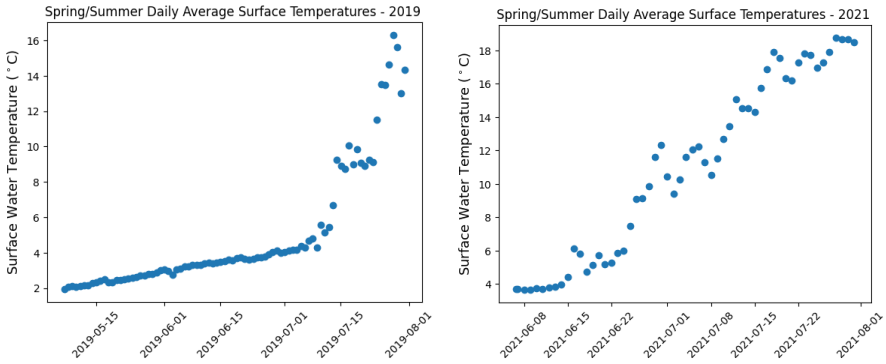

Figure B.1: Individual daily average surface temperatures for the spring-summer periods of each year; Lake Superior site 45006/WM.

A significant gap exists in SWT data between the years 1997-1998. There is none for the year 2020 due to the pandemic.

B.2 Subsurface Water Temperature

Individual plots for each subsurface mooring deployment at WM are shown below.

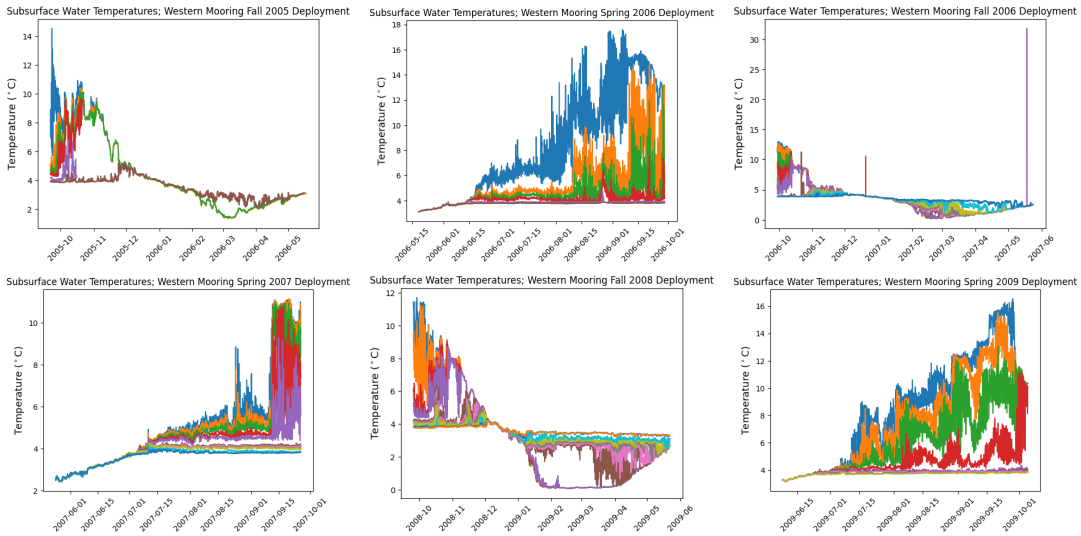

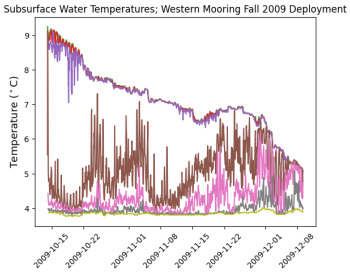
Subsurface Water Temperatures; Western Mooring Fall 2009 Deployment
Temperature (˚C)

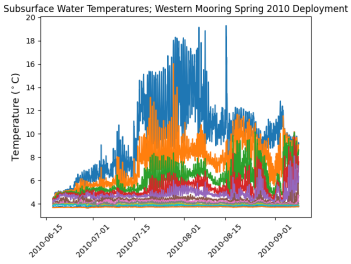
Subsurface Water Temperatures; Western Mooring Spring 2010 Deployment
Temperature (˚C)

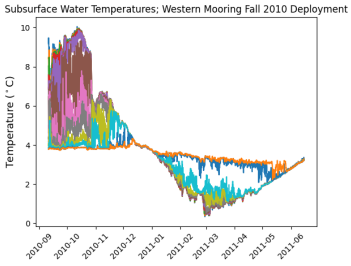
Subsurface Water Temperatures; Western Mooring Fall 2010 Deployment
Temperature (˚C)

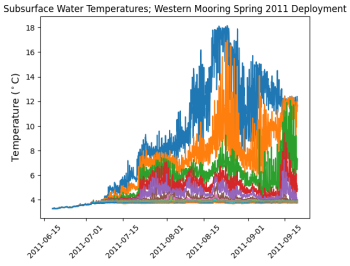
Subsurface Water Temperatures; Western Mooring Spring 2011 Deployment
Temperature (˚C)

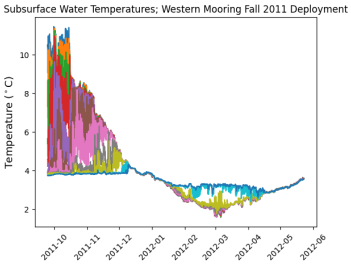
Subsurface Water Temperatures; Western Mooring Fall 2011 Deployment
Temperature (˚C)

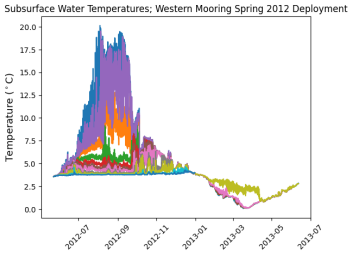
Subsurface Water Temperatures; Western Mooring Spring 2012 Deployment
Temperature (˚C)

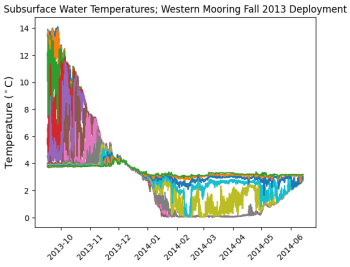
Subsurface Water Temperatures; Western Mooring Fall 2013 Deployment
Temperature (˚C)

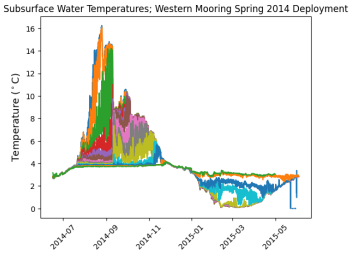
Subsurface Water Temperatures; Western Mooring Spring 2014 Deployment
Temperature (˚C)

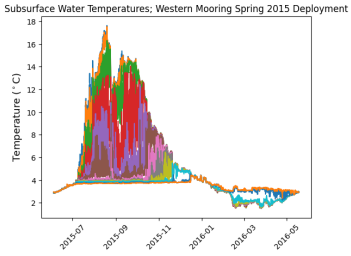
Subsurface Water Temperatures; Western Mooring Spring 2015 Deployment
Temperature (˚C)

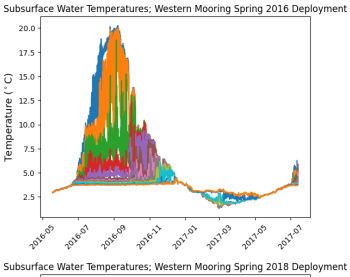
Subsurface Water Temperatures; Western Mooring Spring 2016 Deployment
Temperature (˚C)

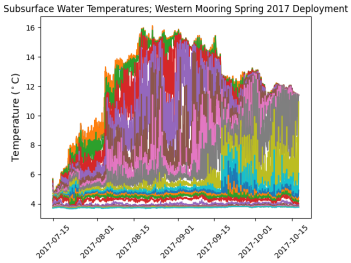
Subsurface Water Temperatures; Western Mooring Spring 2017 Deployment
Temperature (˚C)

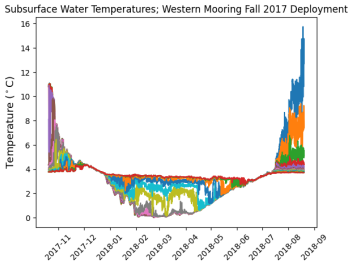
Subsurface Water Temperatures; Western Mooring Fall 2017 Deployment
Temperature (˚C)

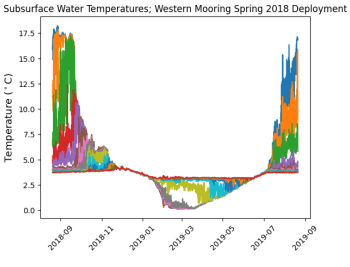
Subsurface Water Temperatures; Western Mooring Spring 2018 Deployment
Temperature (˚C)

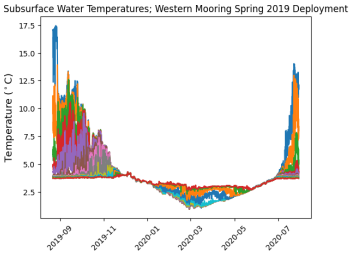
Subsurface Water Temperatures; Western Mooring Spring 2019 Deployment
Temperature (˚C)

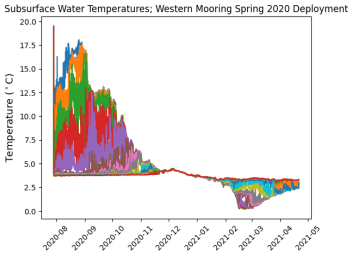
Subsurface Water Temperatures; Western Mooring Spring 2020 Deployment
Temperature (˚C)

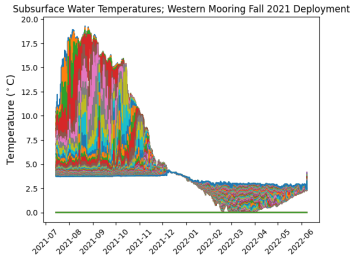

Figure B.2: Individual subsurface water temperature plots for each deployment at the Western Mooring site.

Outlying years of data are:

- 2005

  The first deployment of 2005 used a smaller number of thermistors than future years (6 vs. 15). There is missing data from day 260 onward.

- 2006

  During the second deployment year 2006-2007 there are three spots of bad data from three separate thermistors.

- 2009 Much of 2009 is missing; data is only shown for October-December and it appears only a few thermistors were used.

- 2020

  The initial jump is room temperature data being registered before deployment. This data can be ignored.

- 2021

  The deployment of 2021 utilized far more thermistors than previous years (91). As a result, this is the most accurate year of data.

B.3 Heat Content

Here is shown heat content calculated from SSWT data of 23 deployments spanning the years 2006-2022 at the WM location.

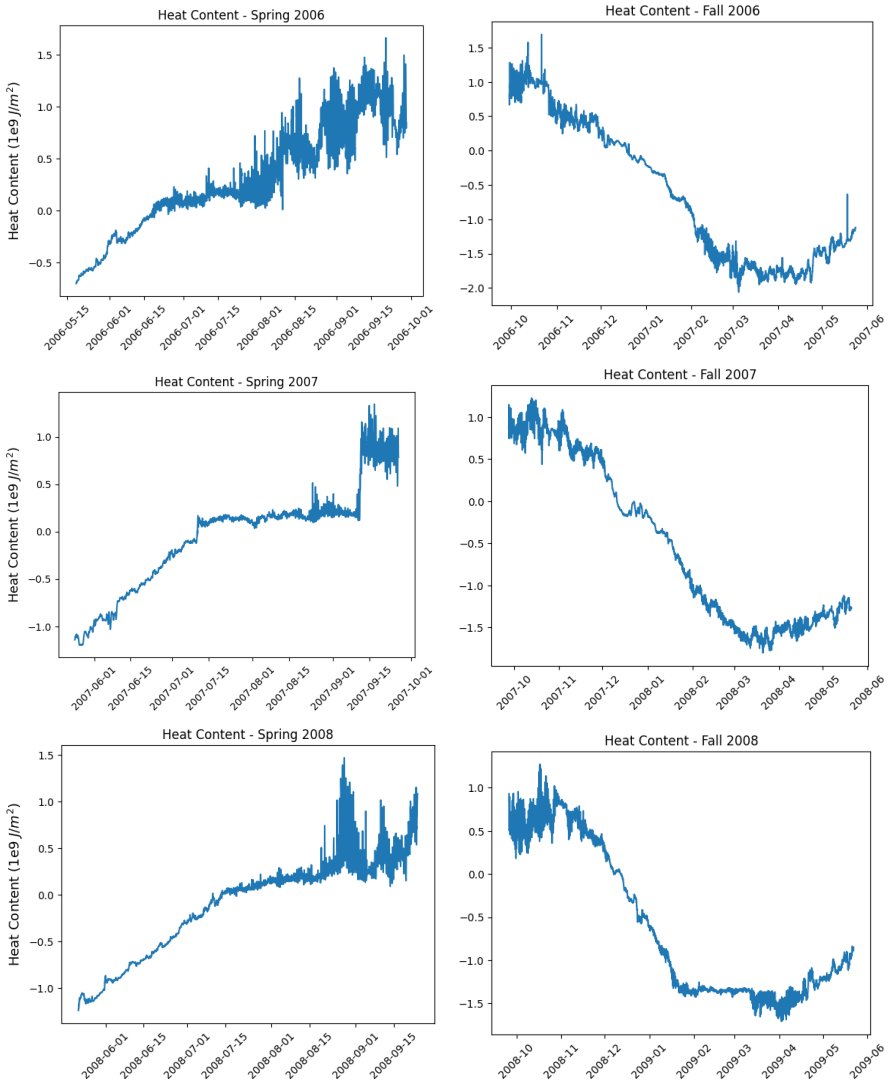

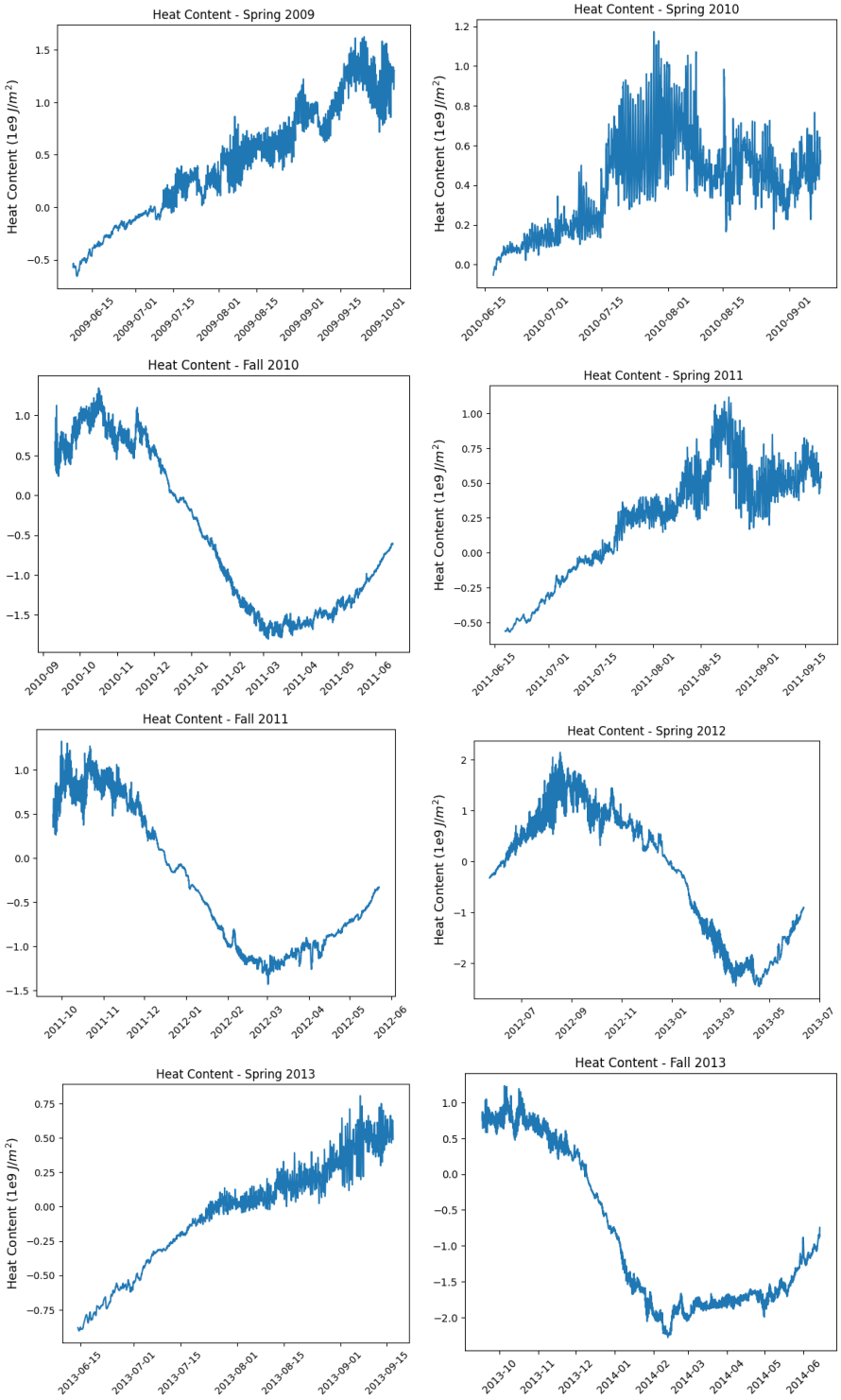
Heat Content - Spring 2009
Heat Content (1e9 J/m²)
2009-06-15
2009-07-01
2009-07-15
2009-08-01
2009-08-15
2009-09-01
2009-09-15
2009-10-01
Heat Content - Spring 2010
Heat Content (1e9 J/m²)
2010-06-15
2010-07-01
2010-07-15
2010-08-01
2010-08-15
2010-09-01
Heat Content - Fall 2010
2010-09
2010-10
2010-11
2010-12
2011-01
2011-02
2011-03
2011-04
2011-05
2011-06
Heat Content - Spring 2011
Heat Content (1e9 J/m²)
2011-06-15
2011-07-01
2011-07-15
2011-08-01
2011-08-15
2011-09-01
2011-09-15
Heat Content - Fall 2011
2011-10
2011-11
2011-12
2012-01
2012-02
2012-03
2012-04
2012-05
2012-06
Heat Content - Spring 2012
Heat Content (1e9 J/m²)
2012-07
2012-09
2012-11
2013-01
2013-03
2013-05
2013-07
Heat Content - Spring 2013
Heat Content (1e9 J/m²)
2013-06-15
2013-07-01
2013-07-15
2013-08-01
2013-08-15
2013-09-01
2013-09-15
Heat Content - Fall 2013
2013-10
2013-11
2013-12
2014-01
2014-02
2014-03
2014-04
2014-05
2014-06

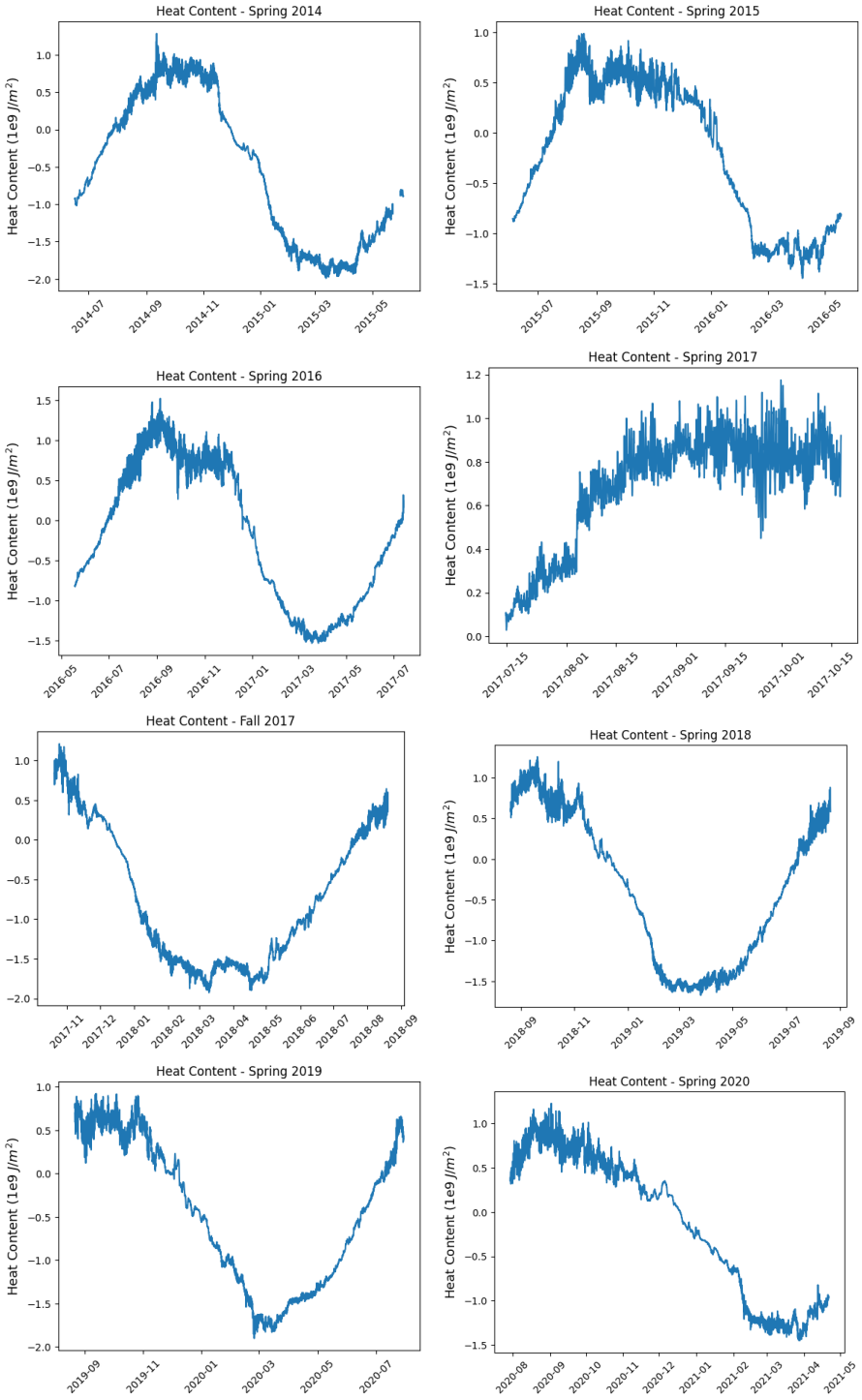
Heat Content - Spring 2014
Heat Content - Spring 2015
Heat Content - Spring 2016
Heat Content - Spring 2017
Heat Content - Fall 2017
Heat Content - Spring 2018
Heat Content - Spring 2019
Heat Content - Spring 2020
Heat Content (1e9 J/m^2)

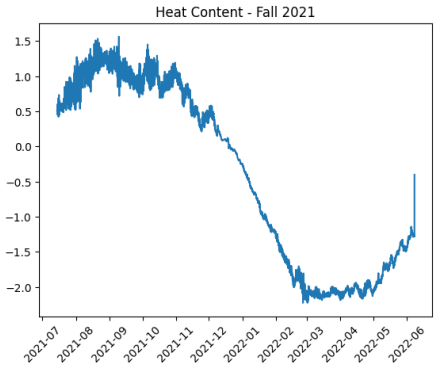

Figure B.3: Heat content calculated from subsurface water temperature profiles for each deployment; Lake Superior Western Mooring.

Appendix C

Tables

C.1 Thermistor arrays

Table C.1: Thermistor depths for each deployment.

Deployment	Thermistors	Depths (m)
Fall 2005	6	17, 25, 30, 36, 70, 120
Spring 2006	6	17, 26, 31, 37, 70, 121
Fall 2006	11	17, 21, 26, 31, 37, 70, 81, 91, 101, 121, 155
Spring 2007	11	17, 20, 25, 30, 36, 70, 80, 90, 100, 120, 155
Fall 2007	11	15, 18, 23, 28, 34, 68, 78, 88, 98, 118, 153
Spring 2008	11	17, 20, 25, 30, 36, 70, 80, 90, 100, 125, 155
Fall 2008	12	17, 20, 25, 30, 36, 70, 80, 90, 100, 120, 155, 173
Spring 2009	9	15, 20, 25, 35, 70, 80, 100, 155, 175
Fall 2009	9	11, 16, 20, 25, 36, 66, 82, 100, 177
Spring 2010	12	11, 15, 20, 25, 30, 40, 50, 60, 81, 100, 150, 177
Fall 2010	12	8, 13, 18, 23, 28, 38, 48, 58, 79, 98, 148, 178
Spring 2011	12	11, 15, 20, 25, 30, 40, 50, 60, 80, 100, 150, 180
Fall 2011	11	15, 20, 25, 30, 40, 50, 60, 81, 100, 150, 180

Continued on next page

Table C.1 – continued from previous page

Deployment	Thermistors	Depths (m)
Spring 2012	11	12, 22, 32, 42, 52, 52, 62, 82, 102, 152, 182
Spring 2013	12	11, 15, 20, 25, 30, 40, 50, 60, 80, 100, 150, 178
Fall 2013	13	9, 15, 20, 25, 30, 40, 50, 60, 81, 100, 125, 150, 180
Spring 2014	13	7, 8, 13, 18, 23, 28, 38, 48, 58, 79, 98, 148, 178
Spring 2015	12	6, 7, 11, 16, 21, 26, 36, 46, 56, 76, 146, 176
Spring 2016	12	10, 15, 20, 25, 30, 40, 50, 60, 81, 100, 150, 180
Spring 2017	20	8, 8, 10.5, 13, 15.5, 18, 20.5, 23, 28, 33, 38, 43, 48, 58, 79, 98, 118, 138, 158, 175
Fall 2017	14	10, 15, 20, 25, 30, 40, 50, 60, 81, 100, 120, 140, 160, 175
Spring 2018	14	7, 8, 13, 18, 23, 28, 38, 48, 58, 79, 98, 148, 178
Spring 2019	14	10, 15, 20, 25, 30, 40, 50, 60, 81, 100, 120, 140, 160, 175
Spring 2020	14	7, 12, 17, 22, 27, 37, 47, 57, 78, 97, 117, 137, 157, 172
Fall 2021	91	12.5, 14, 15.5, 17, 18.5, 20, 21.5, 23, 24.5, 26, 27.5, 29, 30.5, 32, 33.5, 35, 36.5, 38, 39.5, 41, 42.5, 44, 45.5, 47, 48.5, 50, 51.5, 53, 54.5, 56, 57.5, 59, 60.5, 62, 63.5, 65, 66.5, 68, 69.5, 71, 72.5, 74, 75.5, 77, 78.5, 80, 84, 86, 88, 90, 92, 94, 96, 98, 100, 102, 104, 106, 108, 110, 112, 114, 116, 118, 120, 122, 124, 126, 128, 130, 132, 134, 136, 138, 140, 142, 144, 146, 148, 150, 152, 154, 156, 158, 160, 162, 164, 166, 168, 170, 172

C.2 Summer Stratification Dates

Table C.2: Summer Stratification Dates; 1981-2022

Year	Stratification Date
1981	6/23
1982	7/2
1983	7/14
1984	7/14
1985	7/14
1986	6/30
1987	6/17
1988	7/2
1990	7/11
1991	7/7
1992	7/12
1993	7/9
1994	6/30
1995	7/10
1996	7/21
1997	7/15
1999	6/27
2000	6/18
2001	6/29
2002	6/29
2003	7/13
2004	6/30

Continued on next page

Table C.2 – continued from previous page

Year	Stratification Date
2005	6/23
2006	7/5
2008	7/9
2009	6/27
2010	6/8
2011	7/5
2012	6/1
2013	7/16
2014	7/21
2015	7/9
2016	6/19
2017	7/1
2018	7/15
2019	6/29
2021	6/16
2022	7/24